Chapter 10
Adsorption on Solid Surfaces

In previous chapters we have considered two types of interfaces, the solid–vacuum and the solid–solid interfaces. This last chapter is devoted to problems of the solid–gas interface. Some of the questions related to this interface have already been touched on in connection with film growth and the deposition of atoms and molecules to yield a second solid phase and thus a new solid–solid interface. In the present chapter we consider the interaction between a solid surface and foreign atoms in a more fundamental way.

At this point one might ask why the solid–liquid interface is not treated within the framework of the present book. The main reason is a methodological one: Most of the extremely powerful experimental techniques used to study solid–vacuum and solid–solid interfaces in UHV cannot be applied to solid–liquid interfaces, except in extreme cases of monolayer coverage. These, however, are identical with the "adsorption" systems treated in this chapter. Nevertheless great progress has been made recently also in the understanding of solid–liquid interfaces due to the application of optical methods and the powerful scanning tunneling microscopy (STM) techniques described in Panel VI: (Chap. 3).

From a purely theoretical point of view, many features of the solid–liquid interface resemble those of the solid–gas interface. But the plaucity of experimental methods means that our understanding of the solid–liquid interface is less well developed. We thus concentrate here on adsorption processes, i.e. the interaction between a solid surface and atoms or molecules in the gas phase.

10.1 Physisorption

The adsorption of an atom or molecule on a solid surface involves the same basic forces that are known form the quantum-mechanical theory of chemical bonding. Now, however, one of the partners is a macroscopic medium with an "infinite" number of electrons, whose 2D surface is exposed to the other microscopic bonding partner, the atom or molecule. It turns out that many of the concepts of the theory of chemical bonding can be directly transferred to adsorption theory. In particular, there is a clear distinction between physisorption and chemisorption in

H. Lüth, *Solid Surfaces, Interfaces and Thin Films*, 5th ed., Graduate Texts in Physics,
DOI 10.1007/978-3-642-13592-7_10,

the theory of adsorption. Generally speaking, physisorption is a process in which the electronic structure of the molecule or atom is hardly perturbed upon adsorption. The corresponding mechanism in molecular physics is *van der Waals bonding*. The attractive force is due to correlated charge fluctuations in the two bonding partners, i.e. between mutually induced dipole moments. In molecular physics, where these dipoles can be considered as "point" dipoles, the attractive potential is that between attracting dipoles.

In contrast, chemisorption is an adsorption process that resembles the formation of covalent or ionic bonds in molecular physics; the electronic structure of the bonding partners is strongly perturbed, new hybrid orbitals are formed and, as in the case of ionic bonding, there may be charge transfer from one partner to the other. In dissociative chemisorption one may even observe the formation of new molecules.

In spite of the similarity between adsorption and molecular bonding, certain features, such as the variation of forces with distance, might be different due to the different dimensionality of the two problems. Correspondingly one requires different models to describe bonding in molecular physics and in adsorption. This becomes quite clear when one considers a simple model of physisorption. In molecular physics the attractive potential of the van der Waals interaction between neutral molecules can be described by the interaction between mutually induced "point" dipoles. One dipole p_1 formed by momentarily occurring charge fluctuations induces an electric field $\mathcal{E} \propto p_1/r^3$ at the site of the other molecule at distance r. The induced dipole moment there is $p_2 \propto \alpha p_1/r^3$, where α is the polarizability of the molecule. The potential of this dipole p_2 in the field of the first dipole is proportional to $\mathcal{E}$ and to p_2; the attractive part of the van der Waals potential thus has an r^{-6} dependence.

In contrast, the physisorption of a non-reactive atom or molecule (e.g., He, Ne, CH_4) on a solid surface requires a different description [10.1, 10.2]. In Fig. 10.1 the physisorbed atom is modelled by an oscillator in which an electron executes simple harmonic motion (coordinate u) in one dimension. The atom is located outside the surface, which lies at a distance z from the positive nucleus. The van der Waals attraction between the solid and the atom arises from the time-dependent, non-retarded interaction of the valence electron and the nucleus (or core) with their

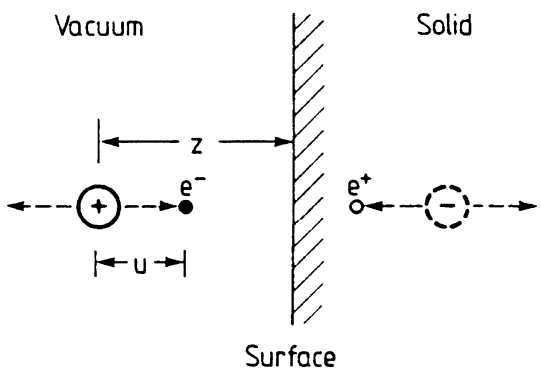

Fig. 10.1 Simple model of a physisorbed atom consisting of a positive ion and a valence electron e^-. The dynamics of the electron is described by a classical oscillation along a coordinate u normal to the solid surface. The attractive interaction with the solid is due to screening, i.e., it arises on forming image charges

images. The van der Waals interaction thus reduces to an image-charge attraction, describable in terms of the screening effects of the solid substrate. A point charge $+e$ outside the surface of a semi-infinite medium with dielectric constant ϵ induces an image point charge.

$$q = \frac{1-\epsilon}{1+\epsilon} e, \tag{10.1}$$

positioned within the medium at the same distance from the surface. For a metal surface ($\epsilon \to \infty$, $q = -e$), the resulting potential energy between the real charge (distance z from surface) and its image is thus $V = -e^2/4\pi\epsilon_0 2z$. Setting $\tilde{q} = e^2/4\pi\epsilon_0$, the interaction energy between nucleus (core), electron and their images is thus obtained as

$$V(z) = -\frac{\tilde{q}^2}{2z} - \frac{\tilde{q}^2}{2(z-u)} + \frac{\tilde{q}^2}{(2z-u)} + \frac{\tilde{q}^2}{(2z-u)}. \tag{10.2}$$

The first term is the interaction of the nucleus (core) with its image, the second arises from the interaction of the electron with its image and the two repulsive terms are the interactions between the nucleus (core) and the electron image and vice versa. Expanding (10.2) in powers of u/z, one finds that terms with z^{-1} and z^{-2} cancel, and that the lowest order, non-vanishing term is

$$V(z) \simeq -\frac{\tilde{q}^2 u^2}{4z^3}. \tag{10.3}$$

The physisorption potential thus depends on the distance z between atom and surface as z^{-3}, in contrast to the r^{-6} dependence of molecular van der Waals bonding. Since the electron wave functions "leak out" of the surface of a metal (or solid in general), the image plane that serves as the reference for the z-coordinate in (10.3) is not identical with the surface itself, i.e. the plane defined by the coordinates of the nuclei of surface atoms. One therefore has to express the lowest-order physisorption potential as

$$V(z) \propto -(z - z_0)^{-3}, \tag{10.4}$$

with z_0 values on the order of half a lattice constant.

Calculations of more accurate physisorption potentials are possible using modern surface band structure and charge-density calculations. But they are tedious and require big computers. Some examples of calculated potential curves $V(z)$ are given in Fig. 10.2 for inert He atoms on Ag, Cu and Au surfaces. The repulsive part, not included in (10.1–10.3) is due to the repulsion of overlapping electron shells, an effect that is included in the realistic calculations. The metal substrates in Fig. 10.2 are described in terms of a jellium model with different mean densities of the smeared-out positive charge. An experimental method for investigating

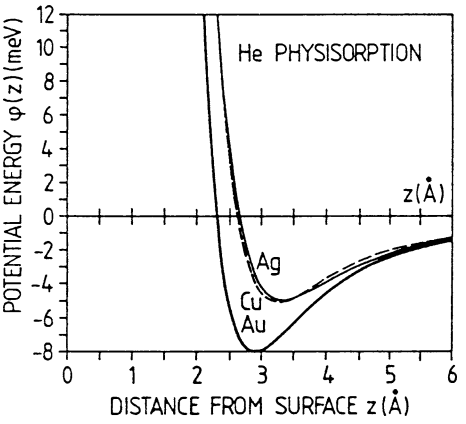

Fig. 10.2 Calculated physisorption potentials $\phi(z)$ for He atoms outside Ag, Cu and Au surfaces. Each metal is described by a jellium model (homogeneously smeared-out charge), in which the properties of the particular metal are accounted for by different mean densities of positive background charge [10.3]

physisorption potentials is based on the analysis of scattering experiments (e.g., He atoms scattered from metal surfaces). The theoretical description of the experimentally determined scattering cross sections and angular distributions allows one to deduce certain features of the interaction potential between surface and scattered particle. Trial and error fits between the measured data and the curves calculated on the basis of assumed potentials yield a best-fit potential.

Physisorption potentials of the type shown in Fig. 10.2 are characterized, in general, by a low binding energy (depth of the potential well) on the order of 10 to 100 meV, and by a relatively large equilibrium separation of 3–10 Å (distance between the potential minimum and the surface $z = 0$).

Physisorbed particles are therefore located at relatively large distances from the surface and are usually highly mobile in the plane parallel to the surface. As with the van der Waals interaction, the binding energy is quite low. Physisorption can only be observed when stronger chemisorption interactions are not present. In general, low temperatures are necessary to study physisorbed species, since at room temperature ($kT \approx 25$ meV) binding in a potential of the type shown in Fig. 10.2 is not possible.

10.2 Chemisorption

Strong adsorbate bonding to a solid substrate must be understood in terms of a chemical reaction, similar to the case of molecular bonding. Covalent adsorption bonds obey essentially the same rules as do covalent bonds between atoms and molecules. The concept of orbital overlap is similarly important, and, for a qualitative approach at least, the same theoretical methods can be used as in the theory of chemical bonding.

In order to demonstrate the general principles underlying chemisorption bonding, let us consider a fairly simple adsorption system (Fig. 10.3), namely a transition metal with an energetically sharp, partially-filled d-band, and a molecule with a

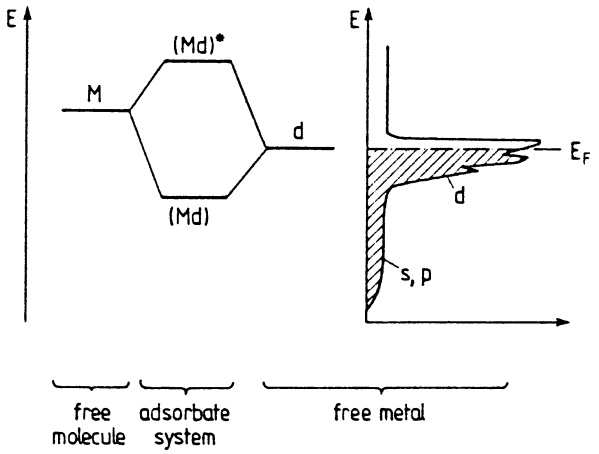

Fig. 10.3 Simple model of covalent chemisorption bonding between a molecule (partially filled molecule orbital M) and a transition metal with partially filled d bands. Bonding with s and p metal states is neglected. In the adsorbate system, bonding (Md) and antibonding $(Md)^*$ states are formed

partially-filled molecular orbital M. When the molecule approaches the metal surface, one expects covalent bonding between the partially filled orbitals of the two partners, i.e., the orbital overlap between M and d should lead to chemisorption with rehybridisation and the formation of new Md orbitals. In a simplified model description we represent the metal d-band by a single energy level (partially filled) and neglect interactions with the s- and p-states of the metal and with molecular orbitals other than M. An approximate wavefunction for the adsorbate-metal system may then be formulated as

$$\psi = a\psi_1(M^-, d^+) + b\psi_2(M^+, d^-), \tag{10.5}$$

where $\psi_1(M^-, d^+)$ and $\psi_2(M^+, d^-)$ represent so-called *charge-transfer states*. $\psi_1(M^-, d^+)$ describes a state in which an electron is transferred from the metal states into the molecular orbital M, whereas $\psi_2(M^+, d^-)$ refers to the reverse situation in which the molecule has donated an electron from its orbital M into the empty part of the metal d-band. The calculation of the new chemisorption energy levels is performed by minimizing the energy functional

$$\tilde{E} = \frac{\langle\psi|\mathcal{H}|\psi\rangle}{\langle\psi|\psi\rangle}. \tag{10.6a}$$

where $\mathcal{H}$ is the total Hamiltonian (molecule plus metal substrate) and ψ as the trial charge-transfer wavefunction (10.5). We define $S = \langle\psi_1|\psi_2\rangle$ as the overlap integral between the two "ionic" charge-transfer states and $H_1 = \langle\psi_1|\mathcal{H}|\psi_1\rangle$ and $H_2 = \langle\psi_2|\mathcal{H}|\psi_2\rangle$ as the total energies of the states in which an electron is transferred from

the metal to the molecule and vice versa. With $H_{12} = H_{21} = \langle\psi_2|\mathcal{H}|\psi_1\rangle$ as the interaction energy between the two "ionic" charge-transfer states (10.6a) becomes

$$\tilde{E}(a^2 + b^2 + 2abS) = (a^2 H_1 + b^2 H_1 + 2abH_{12}). \tag{10.6b}$$

The wave functions ψ_1 and ψ_2 are assumed to be normalized. Minimization of $\tilde{E}$ requires

$$\frac{\partial \tilde{E}}{\partial a} = 0 \text{ and } \frac{\partial \tilde{E}}{\partial b} = 0. \tag{10.7}$$

This yields the secular equations

$$a(\tilde{E} - H_1) + b(S\tilde{E} - H_{12}) = 0, \tag{10.8a}$$

$$a(S\tilde{E} - H_{12}) + b(\tilde{E} - H_2) = 0, \tag{10.8b}$$

whose solutions are given by the vanishing of the determinant

$$\begin{vmatrix} \tilde{E} - H_1 & S\tilde{E} - H_{12} \\ S\tilde{E} - H_{12} & \tilde{E} - H_2 \end{vmatrix} = 0. \tag{10.9}$$

Two energy eigenvalues are obtained from (10.9):

$$\tilde{E}_\pm = \frac{1}{2}\frac{H_1 + H_2 - 2SH_{12}}{1 - S^2} \pm \sqrt{\frac{H_{12} - H_1 H_2}{1 - S^2} + \frac{1}{4}\left(\frac{H_1 + H_2 - 2SH_{12}}{1 - S^2}\right)^2}. \tag{10.10}$$

To demonstrate the qualitative behavior, we assume weak overlap between ψ_1 and ψ_2 and neglect second order terms in S and H_{12} (S^2, H_{12}^2, SH_{12}). In this linear approximation (10.10) yields

$$\tilde{E}_\pm = \frac{H_1 + H_2}{2} \pm \sqrt{\frac{H_1^2 + H_2^2}{2} + H_{12}}. \tag{10.11}$$

Compared to the average ionic energy $(H_1 + H_2)/2$, (10.11) yields two values $\tilde{E}_+$ and $\tilde{E}_-$, which, for positive H_{12}, are respectively higher and lower in energy. They belong to the (Md) chemical bond (Fig. 10.3) and the corresponding antibonding orbital $(Md)^*$. The decrease of the total energy (10.10, 10.11) in $\tilde{E}_-$ favors a chemisorption bond in which electrons are transferred back and forth between adsorbate and substrate. For a more accurate description of the chemisorption bond the ansatz (10.5) for the total wave function is too simple. Better approximations take into account the wave function ψ_0 (*M, met*) of the no-bond state [separated substrate (*met*) and molecule (M), no charge transfer] and charge transfer to all unoccupied metal Bloch states ($k > k_F$, k_F: Fermi wave vector) and from all filled metal states ($k < k_F$) into the molecular orbital M; i.e., instead of (10.5) one uses a trial wave function [10.4]

$$\psi = N\psi_0(M, met) + \sum_{k<k_F} a_k \psi_k(M^-, met^+) + \sum_{k>k_F} b_k \psi_k(M^+, met^-) \tag{10.12}$$

to minimize the energy functional (10.6a).

As in the orbital theory of molecular bonding, the concept of *frontier orbitals* is also useful in a description of chemisorption bonds. The strongest interaction with the adsorbing molecule occurs for an overlap between occupied and unoccupied orbitals, i.e. by electron transfer into the *Lowest Unoccupied Molecular Orbital (LUMO)* and by electron donation from the *Highest Occupied Molecular Orbital (HOMO)* into an empty substrate state. In the simplified picture of Fig. 10.3 LUMO and HOMO are identical, since the highest energy molecular state M carrying a valence electron is assumed to be partially occupied. Carrying out the minimization procedure of (10.6a) by means of (10.12) leads to the equation [10.4]

$$\tilde{E} - E_0 = \sum_{k<k_F} \frac{|U_{Lk}|^2}{E_k - E_{LUMO}} + \sum_{k>k_F} \frac{|U_{Hk}|^2}{E_{HOMO} - E_k} \tag{10.13}$$

for the total energy difference between the bonding situation ($\tilde{E}$) and the non-bonding state (E_0), where the molecule and the substrate are not in contact. E_k are the energies of the unperturbed metal Bloch states (or possibly surface states involved in the bonding); E_{LUMO} and E_{HOMO} are the unperturbed molecular orbital energies, whilst U_{Lk} and U_{Hk} are interaction matrix elements between the metal orbital k and the LUMO ($k < k_F$) and the HOMO ($k > k_F$), respectively.

More sophisticated theoretical approaches to chemical bonding on solid surfaces also exist, but these are far beyond the scope of this book. Particular emphasis to the local nature of a chemisorption bond is provided by cluster models, which are very useful in applying the methods of quantum chemistry to chemisorption bonding. In these calculations the solid surface is modelled by a finite number of substrate atoms (3–20) and the chemisorption bond is described as a chemical bond between this cluster of substrate atoms and the particular chemisorbed atom or molecule. Since the cluster is bonded back to the whole (semi-infinite) solid substrate, it is inert to "backward adsorption". This property is sometimes taken into account by saturating all dangling bonds (apart from the chemisorption bond) with hydrogen atoms.

Chemisorption potentials $\phi(z)$ as a function of the distance z between adsorbate atoms or molecules and the surface are generally characterized by a short equilibrium separation z_0 of 1–3 Å (Fig. 10.4a) and a relatively high binding energy E_B on the order of a couple of eV. Chemisorption is accompanied by a rearrangement of the electronic orbitals, i.e. of the electronic shell of the adsorbate atom or molecule; the shape of the adsorbate is thus changed due to its new chemical bonds to the substrate.

In the case of chemisorption of molecules, this rearrangement of the electronic shell can lead to dissociation and formation of new adsorbate species (Fig. 10.4b).

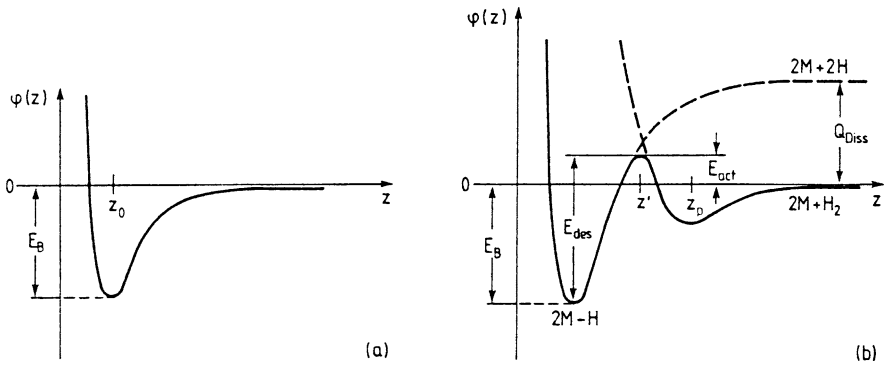

Fig. 10.4 (**a**) Qualitative shape of a chemisorption potential ϕ as a function of the distance z of the adsorbed atom or molecule from the solid surface. The equilibrium distance z_0 is on the order of 1–3 Å and the binding energy E_B on the order of an electron volt. (**b**) Combination of a chemisorption and a physisorption potential shown qualitatively for the example of dissociative hydrogen (H_2) bonding on a metal (M) surface; Q_{Diss} is the dissociation energy of H_2 in the gas phase, E_B is the binding energy in the chemisorption state 2M-H, E_{act} the activation energy for adsorption of H_2, E_{des} the activation energy for desorption of 2H

This so-called *dissociative adsorption* occurs, for instance, for hydrogen molecules on many transition metal surfaces at room temperature. When the clean metal surface is exposed to molecular hydrogen, H_2, rapid adsorption occurs, accompanied by dissociation of the molecules into the atomic species H, which is bonded to the surface. The potential diagram for a hydrogen molecule approaching the surface along a coordinate z (normal to surface) can be described qualitatively as a combination of the potential for physisorption of molecular H_2 and chemisorption of atomic H (Fig. 10.4b). A hydrogen molecule approaching the surface from a large distance z "sees" a potential, which leads into a physisorption state with equilibrium distance z_p (potential minimum). Closer approach to the surface would cause a rapid increase of potential energy due to overlap between the molecule's electronic shell and the metal states. Hydrogen atoms, however, can be bonded on the surface in a chemisorption state with much higher binding energy E_B and a smaller equilibrium distance. The corresponding potential curve for two H atoms differs from that of molecular H_2 at large distances z by exactly the dissociation energy Q_{dis}. This is the energy that must be supplied to dissociation H_2 into 2H in the gas phase.

According to Fig. 10.4b the two potential curves for H_2 and 2H (each time referred to a complete system: two metal atoms (2M) plus hydrogen) intersect at a distance z'. A hydrogen molecule with enough kinetic energy to overcome the activation barrier E_{act} thus prefers to follow the chemisorption potential curve: near z' it is dissociated into two H atoms, which chemisorb on the surface forming two M–H bonds with an adsorption energy E_B. Near z' the electronic structure of the adsorbing particle is completely changed. The molecular orbitals of H_2 transform into atomic orbitals of H. From Fig. 10.4 it is evident that chemisorption of molecular hydrogen into its atomic adsorption state requires a minimum kinetic energy of E_{act},

Table 10.1 Metal ion-binding energies [eV] on different single crystal tungsten surfaces, as determined from experiment [10.5, 10.6]

	Adsorbate			
Substrate	Na	K	Pt	Re
W{100}		2.28	5.0	9.3
W{100}	2.46	2.05	5.5	10.15
W{100}	2.45	2.02		

the activation energy for chemisorption. Since this activation barrier is lower than the dissociation energy Q_{Diss} in the gas phase, dissociation is favored by adsorption on the metal. The decrease of the activation barrier by the presence of a solid surface for dissociation is a feature of catalytic decomposition. From Fig. 10.4 one can also deduce that desorption of chemisorbed atomic H from the metal surface requires a minimum energy E_{des}, the desorption energy. The desorbing H atoms recombine near z' to form molecular H_2, which is detected in the gas phase. For this process of activated adsorption the characteristic energies, E_{B} (chemisorption energy), E_{des} (desorption energy) and E_{act} (activation energy for chemisorption) are related to one another by

$$E_{\mathrm{des}} = E_{\mathrm{B}} + E_{\mathrm{act}}. \tag{10.14}$$

Since particles adsorbed in the chemisorption potential minimum always have a certain finite energy, even at zero temperature, E_{B}, as shown in Fig. 10.4b, must be corrected for this small zero-point energy. Some experimental values of chemisorption binding energies are given in Table 10.1 for metal atoms adsorbed on single crystal surfaces of tungsten. The effect of the d-electrons on the bonding strength for Pt and Re is particularly evident.

10.3 Work-Function Changes Induced by Adsorbates

Adsorbed atoms and molecules generally have a significant influence on the electronic structure of a surface: They rearrange the electronic charge within the chemical bond and may also add elementary dipoles if the adsorbed molecule has its own static dipole moment. It is thus necessary to consider the work function of a solid surface in more detail, in particular in the presence of an adsorbed species.

In previous chapters (Chaps. 6 and 8) the work function $e\phi$ was introduced in an intuitive way as the energy difference between Fermi level E_{F} and the vacuum energy E_{vac}. The precise definition of $e\phi$ is based on a gedanken experiment in which an electron is removed from inside the bulk crystal and transferred through the surface to a region outside, but not too far away from the surface. The distance of the electron from the crystal face should be so large that the image force can be neglected (typically 10^{-4} cm $= 10^4$ Å), but it should be small compared with the distance from any other face of the crystal with a different work function. Otherwise it is not possible to discriminate between work functions of different crystal faces.

In this definition the work function is the energy difference between two states of the whole crystal. As in a photoemission experiment (Sect. 6.3), the initial state is the ground state of a neutral crystal containing N electrons with energy E_N. In the final state one electron is removed to the outside, where it has only electrostatic energy described by the vacuum level E_{vac}. The crystal with the remaining $N-1$ electrons is assumed to be in its new ground state with energy E_{N-1}. We thus obtain for the work function at zero temperature

$$e\phi = E_{N-1} + E_{\text{vac}} - E_N. \tag{10.15}$$

For finite temperatures this process is described as a thermodynamic change of state. The difference $E_N - E_{N-1}$ has to be replaced by the derivative of the free energy F with respect to the electron number (T = const, V = const). This derivative $(\partial F/\partial N)_{\text{T,V}}$ is the electrochemical potential of the electrons (or the Fermi energy E_{F} at finite temperature). A rigorous expression for the work function is thus

$$e\phi = E_{\text{vac}} - \mu = E_{\text{vac}} - E_{\text{F}}. \tag{10.16}$$

Even on a clean, well-defined surface in UHV, the microscopic interpretation of $e\phi$ might contain several contributions. On a metal surface a major contribution is due to the fact that the electron density "leaks out" from the relatively rigid framework of positive ion cores (Fig. 3.7a). This gives rise to a dipole layer at the surface which the emitted electron must pass through. Similar effects occur at steps, which thus also modify the work function of a clean surface (Fig. 3.7b).

In the case of strong chemisorption, charge is shifted from the substrate to the adsorbed atom or molecule, or vice versa, thus giving rise to additional dipoles whose field acts on emitted electrons. This effect is described by a change of the work function $e\Delta\phi$ due to adsorption. Even in the case of physisorption, image charges just below the surface are created (Fig. 10.1) by screening. The resulting dipole moments give rise to work function changes. For semiconductors, one has the additional effect of band bending (Chap. 7), which also contributes to the total work function change (Fig. 10.5). For a semiconductor it is convenient to describe the total work function by means of three terms:

$$e\phi = \chi + eV_{\text{s}} + (E_{\text{C}} - E_{\text{F}})_{\text{bulk}}, \tag{10.17a}$$

where χ is the electron affinity. The effect of dipoles (due to the adsorbed atoms or molecules) $e\Delta\phi_{\text{Dip}}$ is assumed to change the electron affinity from χ to χ', and there is an additional band bending change ΔV_{s}. Thus the total work function change $e\Delta\phi$ of a semiconductor due to adsorption is obtained as

$$e\Delta\phi = \Delta\chi + e\Delta V_{\text{s}} = e\Delta\phi_{\text{Dip}} + e\Delta V_{\text{s}}. \tag{10.17b}$$

The two contributions can be determined separately in a photoemission experiment (Panel XVII: Chap. 10).

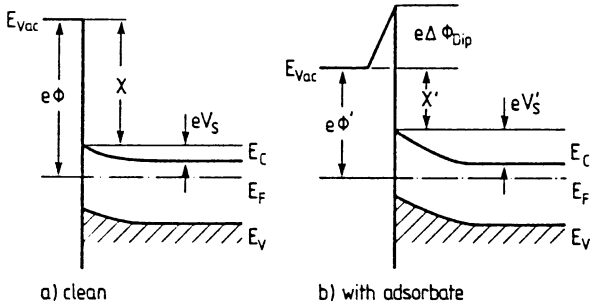

Fig. 10.5 Qualitative electronic-band diagrams of clean and adsorbate-covered semiconductor surfaces; (**a**) clean surface with work function $e\phi$, electron affinity χ, band bending at the surface eV_s, conduction band and valence band edges E_C and E_V; (**b**) chemisorption bonding of an adsorbate generally changes the band bending into $eV_{s'}$; charge transfer within the chemisorption bond induces dipoles within the surface and thus changes the work function and the electron affinity into $e\phi'$ and χ', respectively (dipole contribution $\Delta\phi_{\mathrm{Dip}}$)

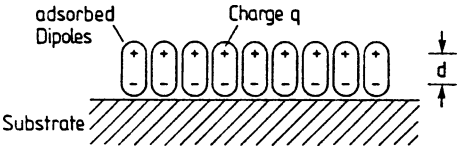

Fig. 10.6 Schematic representation of a well-ordered monolayer of highly-polar molecules with molecular dipole moment qd

The dipole contribution $e\Delta\phi_{\mathrm{Dip}}$ of a monolayer of adsorbate is often calculated on the basis of simplifying assumptions about the nature and magnitude of the dipoles. In a simple model (Fig. 10.6) one can describe the dipole-induced work function change in terms of emitted electrons crossing a parallel plate capacitor (plate separation d), which carries a total charge density $n_{\mathrm{Dip}}q$, n_{Dip} being the surface density of adsorbed dipoles. The corresponding work function change is

$$e\Delta\phi = -q\mathcal{E}d, \tag{10.18}$$

where

$$\mathcal{E} = \frac{n_{\mathrm{Dip}}q}{\epsilon_0} \tag{10.19}$$

is the electric field within the dipole layer (between the capacitor plates). With $p = qd$ as the dipole moment of the adsorbed particle, one has the simple relation

$$e\Delta\phi = \frac{-e}{\epsilon_0} n_{\mathrm{Dip}} p. \tag{10.20}$$

In a more rigorous treatment one has to take into account that the electric field at the site of a particular dipole is modified by all the surrounding dipoles [10.7]. A depolarization effect occurs such that in (10.18) an effective field $\mathcal{E}_{\mathrm{eff}}$ has to be used

$$\mathcal{E}_{\mathrm{eff}} = \mathcal{E} - f_{\mathrm{dep}}\mathcal{E}_{\mathrm{eff}}, \tag{10.21}$$

where f_{dep}, a so-called *depolarization factor*, takes into account the field due to dipoles in the vicinity. According to Topping [10.8], for a square array of uniformly arranged dipoles, this depolarization factor is obtained as

$$f_{\mathrm{dep}} \simeq \frac{9\alpha n_{\mathrm{Dip}}^{3/2}}{4\pi\epsilon_0}, \tag{10.22}$$

where α is the polarizibility of the adsorbed particles (or adsorbate–substrate complexes). From (10.18–10.22) one thus obtains the dipole-induced work function change as

$$e\Delta\phi = -\frac{e}{\epsilon_0} p n_{\mathrm{Dip}} \left(1 + \frac{9\alpha n_{\mathrm{Dip}}^{3/2}}{4\pi\epsilon_0}\right)^{-1} . \tag{10.23}$$

Apart from simple cases such as strong ionic chemisorption, it is difficult to apply (10.23) to real experiments, since neither the dipole moment p nor the polarizability α of the adsorbed particle is well known.

On the other hand, the measurement of work-function changes upon adsorption often yields interesting information about different adsorbed species. Figure 10.7 shows as an example work-function changes $e\Delta\phi$ measured by UPS for a Cu(110) surface which was exposed to H_2O at about 90 K [10.9]. After an initial decrease by about 0.9 eV the work function increases in several steps with increasing temperature. Each step indicates a new adsorbed species which also gives rise to different LEED patterns. The identification of the different species as *physisorbed* H_2O, strongly chemisorbed "H_2O", OH and atomic oxygen (O) was made on the basis of the observed photoemission spectra.

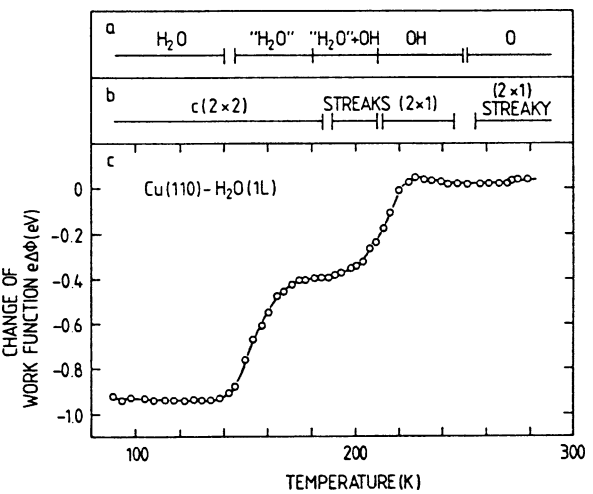

Fig. 10.7 Work-function change $e\Delta\phi$ of a water-covered Cu(110) surface as a function of annealing temperature; the surface was initially exposed to $1\,L = 10^{-6}$ Torr · s of water (**c**); (**a**) adsorbed species as identified by UPS measurement (**b**) corresponding superstructures as observed by LEED [10.9]

In Fig. 10.8 work-function changes measured by UPS on cleaved GaAs (110) are shown as a function of Sb coverage [10.10]. For p- and n-type GaAs completely different curves are obtained, since the band bending contributions $e\Delta V_s$ (10.17) are different. On n-type material the bands are bent upwards due to Sb deposition whereas on p-type material downwards band bending changes are induced. Since the dipole contribution to the work function is related to the microscopic properties of the chemisorption bond, it is assumed to be equal for both dopings. From a more detailed analysis of the data it is found to decrease monotonically up to a coverage of about one monolayer of Sb (Fig. 10.9). This dipole contribution $e\Delta\phi_{\mathrm{Dip}}$ is responsible for the step-like behavior of the total work-function change $e\Delta\phi$ near one monolayer coverage on n-type GaAs (Fig. 10.8a).

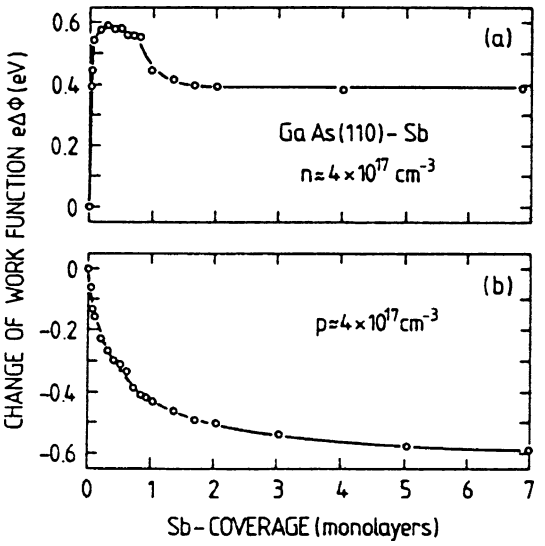

Fig. 10.8 a,b Work-function changes for GaAs(110) surfaces as a function of Sb coverage. (**a**) for n-type material with an electron concentration $n \simeq 4 \cdot 10^{17}\,\mathrm{cm}^{-3}$ with nearly-flat bands prior to deposition of Sb (**b**) for p-type material with a hole concentration $p \simeq 4 \cdot 0^{17}\,\mathrm{cm}^{-3}$ and an initial band bending of -0.3 eV before deposition of Sb [10.10]

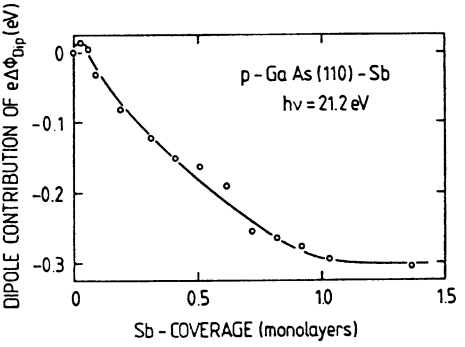

Fig. 10.9 Dipole (electron affinity) contribution $e\Delta\phi_{\mathrm{Dip}}$ to the workfunction change for a GaAs(110) surface due to adsorption of Sb. The data are obtained from UPS measurements on p-doped GaAs surfaces, which exhibited a saturated initial band bending due to irradiation with He II photons before deposition of Sb [10.10]

A particularly interesting system with respect to changes in the work function is the adsorption of cesium both on metal and semiconductor surfaces. Upon adsorption, Cs atoms donate an electron to the substrate and chemisorb as positive Cs^+ with strong ionic chemisorption bonds. A dipole layer with negative charge in the substrate and Cs^+ on the surface is formed. An emitted electron is accelerated within this dipole field on its way from the crystal into the vacuum. The work function is thus considerably decreased by the adsorption of Cs. The effect is demonstrated in Fig. 10.10 for Cs adsorption on different surfaces of W.

On GaAs surfaces the work function or, more specifically, the dipole contribution (i.e., the electron affinity), is reduced by Cs adsorption to such an extent that the vacuum level resides below the conduction band minimum when the additional downwards band bending on *p*-type material is taken into account (Fig. 10.11). The effect is even more pronounced if oxygen is coadsorbed with the Cs atoms. Therefore, any electron which is pumped into the conduction band spills out into the vacuum without having to surmount any energy barrier. GaAs substrates covered with Cs are thus used as high flux sources in electron photoemission. In addition, relativistic effects (spin-orbit splitting) cause the electron states at the top of the valence band to be of such a symmetry that excitation to the conduction band minimum produces free electrons which are highly spin polarized. The additional effect of Cs deposition then allows the fabrication of an effective source of spin polarized electrons.

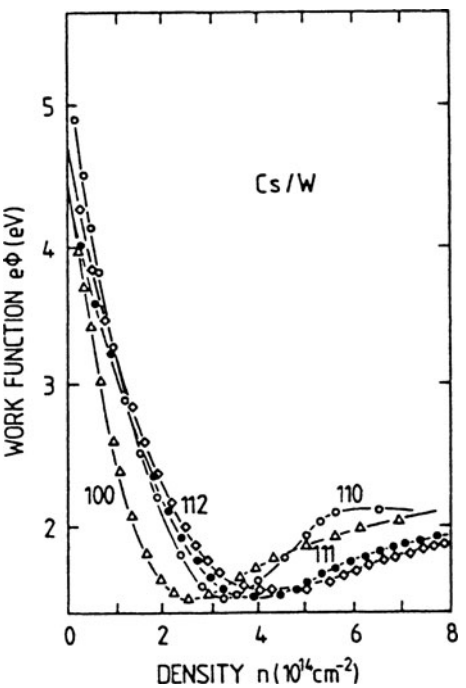

Fig. 10.10 Work function of several tungsten surfaces as a function of coverage with Cs atoms [10.11]

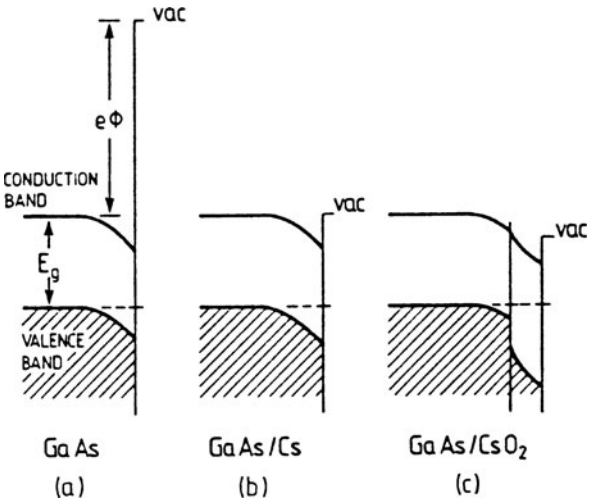

Fig. 10.11 a–c Qualitative band diagram for Cs adsorption on a *p*-type GaAs surface; the dipole contributions are shown in terms of a changed electron affinity. (**a**) clean GaAs surface (**b**) after deposition of Cs (**c**) after coadsorption of Cs and oxygen [10.12]

10.4 Two-Dimensional Phase Transitions in Adsorbate Layers

Figure 10.12 shows the frequencies $\omega_{0\parallel}$ and $\omega_{0\perp}$ of oxygen atoms vibrating parallel and normal to a Ni(100) surface. Atomic oxygen forms a chemisorbed overlayer on Ni(100), which gives rise to a c(2 × 2) superstructure in LEED. The frequencies $\omega_{0\parallel}$ and $\omega_{0\perp}$ have been measured by inelastic scattering of low energy electrons (HREELS) under various scattering angles, i.e. with angular resolution [10.13]. Thus non-negligible wave vector transfer $q_\parallel$ have been obtained and a strong dispersion at least of the $\omega_{0\perp}$ vibration is measured. This dispersion clearly shows – in analogy to the 3D solid – that there is a strong mutual interaction between the atoms forming the ordered 2D array or 2D lattice. Mutual interactions between adsorbed molecules and atoms can also be deduced from the changes in vibration frequency measured (from HREELS or IRS) as a function of coverage. For low coverages, far below a monolayer, interactions within the layer itself cannot be significant. At high coverage in the monolayer range these interactions are important and in analogy to the 3D case one can consider the ordered array of oxygen atoms in Fig. 10.12 as a 2D crystal.

For coverages below a monolayer, two different situations can occur (Fig. 10.13). Case (a), where the adsorbed atoms or molecules are adsorbed in a random and dilute way, can be described in terms of a 2D lattice gas. In Fig. 10.13b the adsorbate layer grows in islands which already possess the internal order of the completed monolayer. This situation can be described as the growth of 2D crystallites. Adsorbate islands with dense packing but with no long-range internal order are described as 2D liquid droplets. Variations of temperature can cause case (b) to change into case (a). This is a 2D phase transition on the surface, in which a 2D crystal or liquid "evaporates" to form a 2D gas.

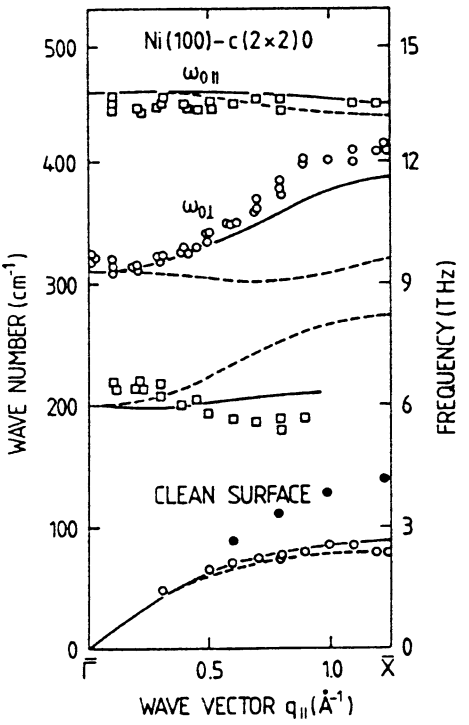

Fig. 10.12 Surface phonon dispersion curves measured on an oxygen covered Ni(100) surface with c(2 × 2) LEED pattern. Full dark circles describe surface phonons of the clean Ni(100) surface. $\omega_{0\parallel}$ and $\omega_{0\perp}$ are vibrational modes of the oxygen atoms with displacements predominantly parallel and normal to the sample surface, respectively [10.13]

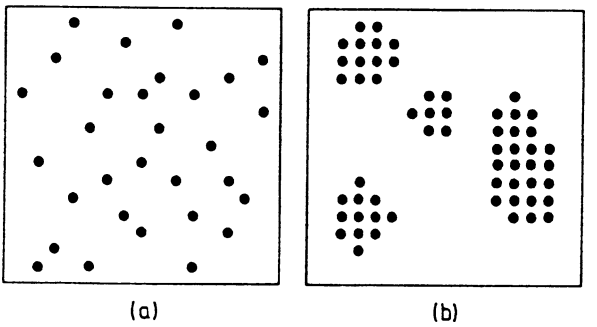

Fig. 10.13 a,b Qualitative representation of 2D adsorbate phases; dots represent adsorbed atoms or molecules. (**a**) random, dilute phase of a 2D gas (**b**) adsorbate islands with 2D internal order, i.e. 2D crystallites

The picture of 2D phases (gas, liquid, solid) of adsorbates appears quite natural where the *vertical* interaction between substrate and adsorbed atoms or molecules is small compared with the "lateral" interaction within the adsorbed layer itself. This case, however, is exceptional: Even for physisorbed layers of inert gas atoms, the van der Waals forces to the substrate can be comparable in strength to those between the adsorbate atoms. In situations of strong chemisorption, the substrate–adsorbate interaction is often much stronger than the lateral interaction. Nevertheless, at elevated temperature, the lateral mobility of the adsorbed species can be considerable and, if the 2D phase is dense enough at higher coverages, the lateral forces cannot be neglected. A description of strongly chemisorbed adsorbates in terms of 2D phase is

also useful to describe lateral order changes, i.e., 2D phase transitions. The *vertical* forces to the substrate, of course, influence the critical parameters (T_c etc.) of such chemisorbed layers. But, in a phenomenological description, these *vertical* forces are not considered explicitly; they are regarded merely as being responsible for establishing the 2D system, i.e., they maintain the adsorbed atoms or molecules in a single plane above the surface.

The relative strength of lateral and vertical interactions also determines whether an ordered adsorbate overlayer (2D crystal) is in or out of registry with the substrate surface periodicity. Strong *vertical* forces impose registry with the surface.

What is the physical nature of the lateral interaction between adsorbed atoms or molecules? Several sources of such interactions might be considered. The most readily identified are:

(i) The *van der Waals attraction*, which is due to correlated charge fluctuations (Sect. 10.1) and is not characteristic for any particular adsorbed atom or molecule. Van der Waals attraction is the only important force for physisorbed inert gas atoms at low temperature. For most other systems, stronger interactions are superimposed and these dominate the net interaction.

(ii) *Dipole forces* may be related to permanent dipole moments of adsorbed molecules (e.g., H_2O, NH_3, etc.) or to the permanent dipoles formed by the adsorption bond due to a charge transfer between substrate and adsorbed atom or molecule. The interaction between parallel dipoles is, of course, repulsive.

(iii) *Orbital overlap* between neighboring atoms or molecules in a densely packed adsorbate layer also leads to a repulsive interaction. The behavior of CO at high coverages on transition metals is most probably dominated by this type of interaction.

(iv) *Substrate-mediated interactions* can have two origins. A strongly chemisorbed atom or molecule modifies the substrate electronic structure in its vicinity due to the chemisorption bond. A depletion or accumulation of charge in the substrate over distances of a few Ångstroms can increase or decrease the interaction strength with a second adsorbate particle and may therefore cause an indirect interaction between the adsorbate atoms or molecules.

A similar interaction can be mediated through the elastic properties of the substrate. A strongly chemisorbed atom might attract substrate atoms in its neighborhood due to the strong charge rearrangement. There is thus a local contraction of the lattice which must be compensated by an expansion at more distant points. Suppose a second adsorbate atom also attracts the substrate atoms. This second adsorbate has to do more work in order to contract the lattice at adsorption sites with lattice expansion than at those that are already contracted. Thus, depending on their separation, a repulsive or attractive interaction can arise between the adsorbate atoms. The indirect substrate-mediated lateral interactions are usually weaker than the direct dipole–dipole interactions.

As in the case of 3D solids, information about the interaction forces can be deduced from a study of phase transitions and critical parameters such as critical

temperature T_c, pressure p_c, and density n_c. Via the equation of state, these parameters determine the conditions for phase transitions. A whole variety of equations of state are possible for a 2D system [10.14], but we restrict ourselves here to the simplest type of equation, the van der Waals equation. For 3D systems this reads

$$(p + an^2)(1 - nb) = nkT. \tag{10.24}$$

This is the simplest and most plausible semi-empirical formula for the description of a non-ideal fluid in the liquid–vapor regime. n is the volume density of particles ($n = N/V$), and b is the volume of a particle, i.e. the volume which is excluded for another particle. For interparticle potentials that are not of the hard-core type, a is given approximately by $4\pi R^3/3$, where R is the separation at which strong repulsion between particles becomes important. The constant b takes into account the (two-body) interparticle potential $\phi(r)$ between two atoms or molecules at distance r. Within the approximations involved in deriving the van der Waals equation [10.14], a is given in terms of the interparticle potential $\phi(r)$ by

$$\frac{a}{V} = -\frac{N}{2}\int_{2R}^{\infty} \phi(r)\frac{N}{V}4\pi r^2 \mathrm{d}r, \tag{10.25}$$

where N is the number of particles and V the corresponding volume. The parameter a is essentially the total potential energy due to attractive interactions with other particles in the neighborhood of the one considered.

The simplest equation of state that allows a rough description of the phase transition 2D gas $\rightleftharpoons$ 2D liquid is obtained be rewriting (10.24, 10.25) in two dimensions. The thickness of the quasi-2D system, i.e., of the adsorbed layer, is $d(= 1\text{–}3\,\text{Å})$. With θ as the area density of particles (number per cm^2) one has

$$nd = \theta; \tag{10.26}$$

and with f_p as the minimum area that has to be attribute to one particle, it follows that

$$b = df_p. \tag{10.27}$$

For the 2D problem one has to introduce a so-called *splay pressure*, π, which is defined as the force acting on a line element, i.e., for the present system π is related to the usual pressure p by

$$\pi = dp. \tag{10.28}$$

Using (10.26–10.28) one obtains from (10.24) the van der Waals equation for a 2D adsorption system:

$$\left(\pi + \frac{a\theta^2}{d}\right)\left(\frac{1}{\theta} - f_p\right) = kT. \tag{10.29}$$

Instead of using the absolute area density θ one often refers to the relative coverage θ_r which is related to the coverage θ_0 of a completed monolayer by $\theta_r = \theta/\theta_0$.

The van der Waals isotherms $\pi(\theta, T = \text{const.})$ describing a 2D liquid-gas system (Fig. 10.14) are essentially identical to those of a normal 3D liquid-gas system. For temperatures below a critical temperature T_c, there is a certain surface-density range between A and B, where the liquid and the gaseous adsorption phases coexist on the surface. For θ^{-1} above A only the less dense gaseous phase of the adsorbate is present, whereas for θ^{-1} below B the adsorbate is in its more dense liquid phase. For temperatures higher than the critical temperature there is no distinction between the liquid and the gas phase. The thermal kinetic energy is so high that "condensation" cannot occur; the splay pressure π is correlated monotonically with the surface density θ. This property of the gas-liquid system is also obvious from a temperature versus density (or T versus θ^{-1}) plot (Fig. 10.15). If one plots the densities θ (or θ^{-1}) at which the transitions gas-coexistence phase (point A in Fig. 10.14) and coexistence phase-liquid (point B in Fig. 10.14) occur, as a function of temperature, a phase diagram as shown in Fig. 10.15 is obtained. Below T_c liquid and gas phases are separated by the coexistence regime. For temperatures higher than T_c the transition from gas to liquid is continuous and there is no real phase separation between the two.

For the simple van der Waals equation of state (10.29), the critical parameters, temperature T_c, density θ_c, and splay pressure π_c are obtained by finding that

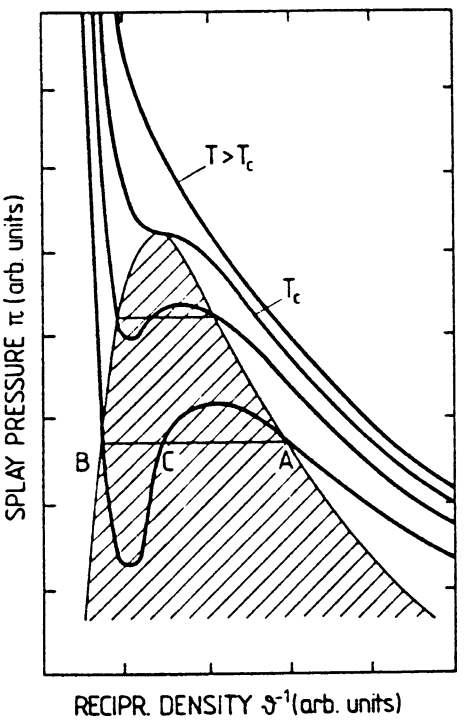

Fig. 10.14 Qualitative 2D liquid-gas phase diagram (isotherms) for an adsorbate system forming dense liquid-like and dilute gas-like structures on the surface. Above the critical temperature T_c only the 2D gas phase exists, below T_c gaseous and liquid phases coexist for reciprocal densities θ^{-1} between A and B

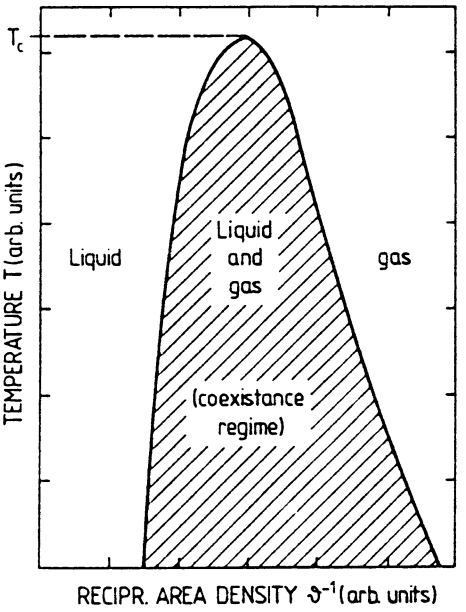

Fig. 10.15 Qualitative 2D phase diagram for an adsorbate that exists both as a 2D liquid and as a 2D gas on the surface. The coexistence curve with enclosed coexistence regime (shaded) is plotted in the plane of substrate temperature T versus reciprocal area density θ^{-1} of the adsorbed particles. T_c is the critical temperature above which a distinction between liquid and gas is no longer possible

solution of the cubic equation (10.29) for which all three roots θ_c coincide. For this particular θ_c, (10.29) represented as

$$\theta^3 - \frac{1}{f_p}\theta^2 + \left(\frac{\pi d}{a} + \frac{d}{af_p}kT\right)\theta - \frac{\pi d}{af_p} = 0 \tag{10.30}$$

must become

$$(\theta - \theta_c)^3 = \theta^3 - 3\theta_c\theta^2 + 3\theta_c^2\theta - \theta_c^3 = 0. \tag{10.31}$$

By comparison of the θ^n coefficients one obtains

$$3\theta_c = 1/f_p, \tag{10.32}$$

$$3\theta_c^2 = \left(\frac{\pi_c d}{a} + \frac{d}{af_p}kT_c\right) \tag{10.33}$$

$$\theta_c^3 = \frac{\pi_c d}{af_p}. \tag{10.34}$$

This yields the following critical parameters

$$\theta_c = \frac{1}{3f_p}, \tag{10.35}$$

$$\pi_c = \frac{a}{27df_p^2}, \tag{10.36}$$

$$T_c = \frac{8}{27}\frac{a}{kdf_p}. \tag{10.37}$$

An experimental evaluation of the critical parameters, temperature T_c, splay pressure π_c, and critical density θ_c, thus gives direct insight into the interesting interaction parameters f_p (minimum particle area) and the total interaction energy a between one particle and its neighbors (10.25).

Simple 2D phase diagrams, as shown qualitatively in Fig. 10.15, are indeed found for certain adsorption systems. Atomic hydrogen (H) on Ni(111) can form an ordered, *crystalline* phase with a (2×2) superstructure seen in LEED [10.15]. But the occurrence of this structure is critically dependent on the coverage and the

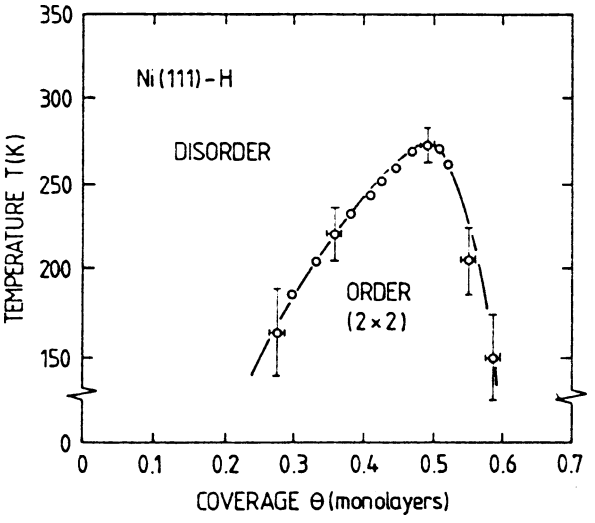

Fig. 10.16 Experimental 2D phase diagram for atomic hydrogen adsorbed on Ni(111). Depending on the coverage θ and substrate temperature T, one may observe an ordered adsorbate phase with (2×2) superstructure or a disordered phase [10.15]

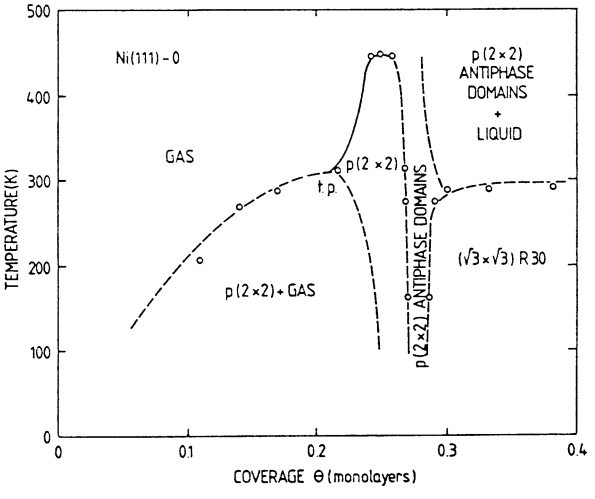

Fig. 10.17 Experimental phase diagram (○) and a postulated phase diagram for the oxygen on Ni(111) system; continuous phase boundaries are shown as solid lines, first order phase boundaries as dotted lines, t.p. is the tricritical point [10.16]

substrate temperature. A phase diagram $T_c(\theta)$ can be determined experimentally by LEED studies (Fig. 10.16), and this indeed shows the qualitative features of a simple van der Waals phase diagram (Fig. 10.15).

For other systems, e.g. oxygen on Ni(111), more complex phase diagrams have been observed experimentally (Fig. 10.17). In addition to the random gas and liquid states, several 2D crystalline states exist. These exhibit various characteristic superstructures, such as p(2 × 2) or $(\sqrt{3} \times \sqrt{3})$R30°.

10.5 Adsorption Kinetics

So far we have discussed the microscopic details of single adsorbed molecules or atoms and the structure and properties of the adsorbed phase. In order to analyse a real adsorption experiment, a more phenomenological framework is needed to describe measured quantities such as adsorption rate and degree of coverage. So far we have considered properties of the adsorption system in thermal equilibrium; in contrast, the description of adsorption and desorption rates requires non-equilibrium considerations related to adsorption kinetics. These quantities depend, of course, on the details of the particular adsorption process, but their relationship to the microscopic picture is often complex and not well understood. Nevertheless, the *kinetic description* on a more phenomenological level can yield first important information, which, in combination with more refined spectroscopic data, can lead to a deeper understanding of adsorption interactions.

Adsorption kinetics is a thermodynamic approach describing the interplay between the adsorbed species and the ambient gas phase; adsorption and desorption are the two processes which determine the macroscopic coverage on a solid surface exposed to a gas. The adsorption rate depends on the number of particles striking the surface per second and on the so-called *sticking coefficient*, which is the probability that an impinging particle actually sticks to the substrate. According to kinetic gas theory (Sect. 2.1) the rate at which particles impinge on a surface (per unit area and time) is given by

$$\frac{\mathrm{d}N}{\mathrm{d}t} = \frac{p}{\sqrt{2\pi mkT}}. \tag{10.38}$$

The adsorption rate, i.e. the number of adsorbing particles per unit time and surface area is then obtained as

$$u = S\frac{\mathrm{d}N}{\mathrm{d}t} = S\frac{p}{\sqrt{2\pi mkT}}, \tag{10.39}$$

where m is the mass of the impinging particle.

Since the coverage θ (number of adsorbed particles per unit area) is given by

$$\theta = \int u\mathrm{d}t = \int S\frac{\mathrm{d}N}{\mathrm{d}t}\mathrm{d}t, \tag{10.40}$$

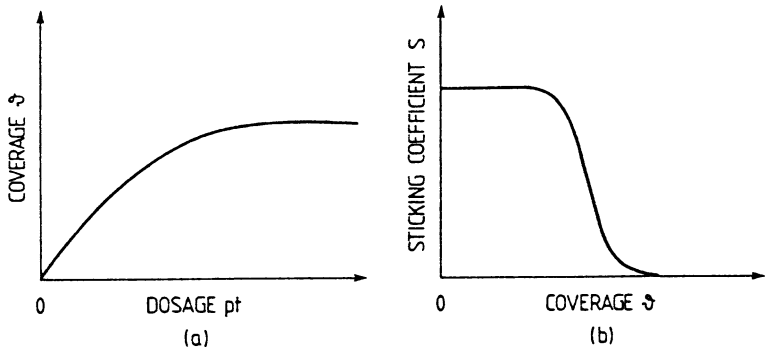

Fig. 10.18 (**a**) Qualitative dependence of coverage θ on exposure (**b**) corresponding dependence of the sticking coefficient S on coverage θ

one can determine the sticking coefficient S from a measurement of the coverage θ (e.g., by AES) as a function of dosage (Fig. 10.18).

According to (10.38, 10.40) one has

$$S = \sqrt{2\pi mkT}\frac{u}{p} = \sqrt{2\pi mkT}\frac{1}{p}\frac{\mathrm{d}\theta}{\mathrm{d}t}. \tag{10.41}$$

Typical coverage versus dosage (pressure-time) dependences, as shown in Fig. 10.18a, yield, after differentiation, a sticking coefficient $S(\theta)$ as in Fig. 10.18b. The general shape of the $S(\theta)$ dependence is easy to understand on the basis that the first chemisorbed molecules or atoms bond to "free" valence orbitals (dangling bonds) of the surface and thus decrease its reactivity to further bonding as more and more sites become occupied. The sticking coefficient S implicitly reflects the details of the microscopic adsorption process. Several important factors affect the quantity S:

(i) In many cases (e.g., see Fig. 10.4b) an activation barrier E_{act} has to be overcome before chemisorption can occur. Only atoms or molecules whose impact energy exceeds E_{act} can stick to the surface. In this case of activated adsorption the sticking coefficient must contain a Boltzman term $\exp(-E_{\mathrm{act}}/kT)$.

(ii) In order for an impinging atom or molecule to be chemisorbed, its electronic orbitals must have a particular orientation with respect to the dangling-bond orbitals of the surface (steric factor). Besides the orientation of the molecules, their mobility on the surface and the site of impact are also important. The adsorption potential varies locally along the surface due to the atomic structure of the substrate.

(iii) During adsorption, an incident atom or molecule must transfer at least part of its remaining kinetic energy to the substrate, otherwise it will be desorbed again after approximately one vibrational period. Excitations of the substrate, such as surface phonons, and plasmons, are thus also involved in the adsorption kinetics.

(iv) Adsorption sites must of course be available to an impinging atom or molecule. The more sites are occupied, the fewer particles can be adsorbed. For particles adsorbed in a precursor (intermediate) state, the diffusion path to a final sticking site becomes longer; this enhances the probability of desorption and decreases the sticking probability.

A convenient description of the sticking coefficient for activated adsorption, taking into account the above-described phenomena, is thus

$$S(\theta) = \sigma f(\theta) \exp(-E_{\text{act}}/kT), \tag{10.42}$$

where σ, the so-called *condensation coefficient* contains the effects of molecular orientation (steric factor), energy transfer to the surface, etc. $f(\theta)$ is the occupation factor, which describes the probability of finding an adsorption site. For non-dissociative adsorption (mobile or immobile adsorption) a site is occupied or unoccupied and $f(\theta)$ is simply

$$f_1(\theta) = 1 - \theta, \tag{10.43}$$

where θ is now the relative coverage, i.e., the ratio between occupied sites and the maximum number of available sites in the first completed adsorbed layer. For dissociative adsorption, where the impinging molecule dissociates into e.g. two adsorbed radicals, the second radical must find an empty site directly neighboring the first radical, at least for an immobile adsorbate. With z as the maximum number of adjacent sites for the second radical, the number of available sites is

$$f_2(\theta) = \frac{z}{z - \theta}(1 - \theta). \tag{10.44}$$

For adsorption of the whole molecule, i.e. two immobile radicals one obtains

$$f(\theta) = f_1(\theta) f_2(\theta) = \frac{z}{z - \theta}(1 - \theta)^2. \tag{10.45}$$

For low coverages ($\theta \ll 1$) one has

$$f(\theta) \simeq (1 - \theta)^2. \tag{10.46}$$

This expression is, of course, also valid for dissociative adsorption of mobile complexes, since, for low enough coverage, sufficient sites are free that there is no real restriction due to prior occupation of neighboring sites. The condensation coefficient σ depends on the various states in which the adsorbed molecule, the free gas phase molecule and the adsorbant surface can exist. A detailed statistical theory [10.17] for the calculation of σ describes the adsorption process as a transition from the initial state of the free surface plus free molecule $(S + M)$ via an excited transition state $(SM)^*$ into the final adsorption state (SM). In the transition state $(SM)^*$ the system

is in a state of excitation, its total energy includes the activation energy which has to be supplied before adsorption occurs. Adsorption may thus be considered as the decay of the transition state into the adsorption state. Rate theory then yields the result that σ is given essentially by the ratio

$$\sigma \propto Z_{(\mathrm{SM})^*}/Z_{\mathrm{M}}Z_{\mathrm{S}}, \tag{10.47}$$

where Z are the partition functions of the excited transition complex $(\mathrm{SM})^*$, of the free molecule (M) and the free surface (S).

These partition functions are sums over the various possible states, e.g. for a molecule with energy eigenvalues ϵ_i (degree of degeneracy g_i) one has

$$Z_{\mathrm{M}} = \sum_{\mathrm{i}} g_\mathrm{i} \exp(-\epsilon_\mathrm{i}/kT). \tag{10.48}$$

The calculation of σ for a realistic system clearly requires a detailed knowledge of the reaction path and of the quantum-mechanical properties of the various constituents. Table 10.2 gives some characteristic values for simple diatomic gases in both mobile and immobile adsorbate layers. σ is dependent mainly on the degree of freedom of the adsorbed molecule.

Experimentally, one sometimes finds an exponential dependence of the sticking coefficient S on the coverage θ:

$$S \propto \exp(-\alpha\theta/kT) \tag{10.49}$$

(Elovich equation). This dependence is easily understood according to (10.42), if the activation energy E_{act} is assumed to depend on coverage as $E_{\mathrm{act}} = E_0 + \alpha\theta$.

The *desorption process* is described phenomenologically by a desorption rate υ, i.e. the number of desorbing particles per unit time and surface area. For desorption to occur, an adsorbate particle must acquire enough energy to surmount the desorption barrier $E_{\mathrm{des}} = E_{\mathrm{B}} + E_{\mathrm{act}}$, which comprises the binding energy E_{B} and the activation energy for adsorption (Fig. 10.4b). The desorption rate υ is thus proportional to the exponential term $\exp(-E_{\mathrm{des}}/kT)$, but as for adsorption, the number of adsorbed particles also enters via an occupation factor $\overline{f}(\theta)$, as do the detailed steric and mobility factors by means of a desorption coefficient $\overline{\sigma}(\theta)$. The quantities $\overline{f}(\theta)$ and $\overline{\sigma}(\theta)$ describe a process which is inverse to adsorption; accordingly they

Table 10.2 Some characteristic condensation coefficients σ for diatomic molecules adsorbed in mobile and immobile configurations [10.17]

Adsorbate	Immobile adsorbate	Mobile adsorbate	
		loss of rotation	no loss of roation
H_2	$3 \cdot 10^{-2}$–0.2	0.52	1
O_2, N_2	10^{-4}–$3 \cdot 10^{-2}$	0.12	1
CO_2	$7 \cdot 10^{-5} - 0.02$	0.1	1

are complementary to f and σ, i.e. inversely dependent on coverage and on the partition functions of adsorbate, substrate and transition complex. In the simplest case of desorption of one atom from a single site, one has

$$\overline{f}(\theta) = \theta. \tag{10.50}$$

In the case of a molecular process where the desorbing molecule originates from two radicals at different sites, there is an approximate dependence

$$\overline{f}(\theta) \simeq \theta^2. \tag{10.51}$$

As a whole, the desorption process is described by a desorption rate

$$v = \overline{\sigma}(\theta)\overline{f}(\theta)\exp(-E_{\mathrm{des}}/kT). \tag{10.52}$$

Thermal equilibrium between the gas phase and the solid surface is characterized by equal adsorption and desorption rates. At a constant temperature, there thus exists an equilibrium adsorbate coverage $\theta(p, T)$, which is described by the so-called *adsorption isotherm*. To calculate this, one equates the adsorption and desorption rates u and v:

$$u = v. \tag{10.53a}$$

With the simple assumptions of (10.42 and 10.52) one thus obtains

$$u = \sigma(\theta) f(\theta) \mathrm{e}^{-E_{\mathrm{act}}/kT} \frac{p}{\sqrt{2\pi mkT}} = \overline{\sigma}(\theta)\overline{f}(\theta)\mathrm{e}^{-E_{\mathrm{des}}/kT} = v, \tag{10.53b}$$

or, with $E_{\mathrm{des}} = E_{\mathrm{B}} + E_{\mathrm{act}}$

$$p = \frac{\overline{\sigma}}{\sigma}\sqrt{2\pi mkT}\mathrm{e}^{-E_{\mathrm{B}}/kT}\frac{\overline{f}(\theta)}{f(\theta)} = \frac{1}{A}\frac{\overline{f}(\theta)}{f(\theta)}. \tag{10.54}$$

This is the general form of the so-called *Langmuir isotherm*. For the special case of non-dissociative adsorption (10.43), where $f(\theta) = 1 - \theta$ and $\overline{f}(\theta) = \theta$ one obtains the simple form

$$p(\theta) = \frac{\theta}{A(1-\theta)}, \quad \text{or} \quad \theta(p) = \frac{Ap}{1+Ap}, \tag{10.55}$$

where A is a constant at a fixed temperature, see (10.54). A measurement of the equilibrium adsorbate coverage θ as a function of ambient pressure p therefore allows a determination of the constant A, which in turn yields, according to (10.54), the chemisorption (or binding) energy E_{B}, provided the condensation and desorption coefficients σ and $\overline{\sigma}$ are known. Figure 10.19 shows the qualitative dependence of

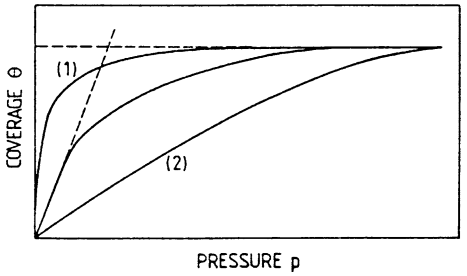

Fig. 10.19 Qualitative shapes of Langmuir-type isotherms of coverage versus pressure $\theta(p)$. Curve (1) describes the case of strong adsorption with large adsorption energy, curve (2) represents the case of weak adsorption. Between these extremes there is a gradual transition from type (1) to (2)

coverage θ on pressure p as expected from the Langmuir isotherm (10.55). For low pressures, the curves can be approximated by a linear relationship whose slope ($\simeq A$) increases exponentially with adsorption energy E_B, i.e. with the strength of the adsorption process.

For many realistic adsorption systems the Langmuir isotherm fails to correctly describe the dependence of coverage on pressure in thermal equilibrium. In particular, the neglect of multilayer adsorption is unrealistic. Much better agreement was achieved by a theory of Brunauer, Emmett and Teller (BET isotherm), in which multilayer adsorption was also taken into account. Each adsorbed particle in the first layer serves as a site for adsorption into the second layer, and each particle in the second layer serves as a site for adsorption into the third layer and so forth. In even more refined approaches, activation energy, adsorption energy, etc., are assumed to be layer dependent. In this way more parameters enter into the theory, but a variation of these parameters allows an accurate description of a variety of experimentally observed isotherms (Fig. 10.20).

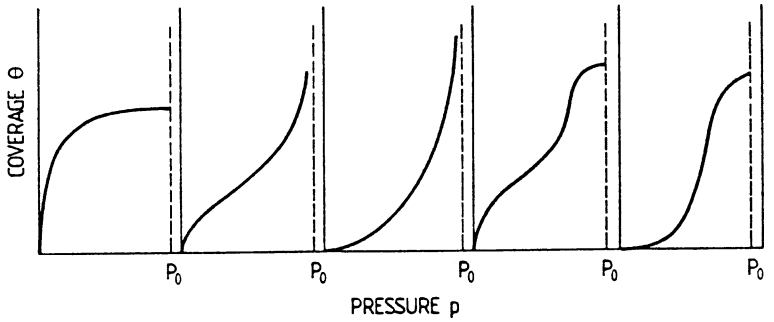

Fig. 10.20 Various possible physical adsorption isotherms

Panel XVI
Desorption Techniques

Much essential information about adsorption processes and surface chemical reactions is derived from desorption experiments. The entire class of desorption techniques has the common feature that a clean surface under UHV conditions is exposed to a well-defined gas atmosphere or a molecular beam. Subsequent desorption of the resultant adsorbate is performed by thermal annealing of the surface or by irradiating with light or energetic particles. The desorbing species can be analysed mass-spectroscopically or the particle beam can be optically imaged on a screen to yield information about possible anisotropy in the angular distribution of the desorbing atoms or molecules.

The simplest technique which gives useful information, particularly about simple adsorption systems, is the so-called *Thermal Desorption Spectroscopy* (TDS), where thermal annealing of the adsorbate-covered surface gives rise to desorption [XVI.1]. A straightforward measurement of the pressure increase in the UHV chamber as a function of sample temperature yields interesting information about the desorption energy, etc. The mathematical description of the desorption process is based on the pumping equation (I.2). The desorbing particles are pumped away (pumping speed $\tilde{S}$) but give rise to a temporary pressure increase in the UHV vessel. With v as the desorption rate, particle conservation thus yields

$$vA = \frac{-A\mathrm{d}\theta}{\mathrm{d}t} = \frac{V_\mathrm{v}}{kT}\left(\frac{\mathrm{d}p}{\mathrm{d}t} + \tilde{S}\frac{p}{V_\mathrm{v}}\right), \tag{XVI.1}$$

where θ is the relative coverage of the sample surface (area A), V_v the volume of the UHV chamber and p the pressure (background subtracted).

In the limit of negligible pumping speed the rate of the pressure increase would reflect the desorption rate ($\mathrm{d}\theta/\mathrm{d}t \propto \mathrm{d}p/\mathrm{d}t$). On the other hand, with modern pumping equipment $\tilde{S}$, is extremely high (for cryopumps $\tilde{S}$ can reach values of 10 000ℓ/s and (XVI.1) can be approximated by

$$v = \frac{-\mathrm{d}\theta}{\mathrm{d}t} \propto p, \tag{XVI.2}$$

such that monitoring the pressure directly yields interesting information about the desorption rate. The desorption rate might be described as in (10.52) by means of

$$v = \frac{-\mathrm{d}\theta}{\mathrm{d}t} = \overline{\sigma}\,\overline{f}(\theta)\exp(-E_{\mathrm{des}}/kT), \tag{XVI.3}$$

with E_{des} as the desorption energy. In the simplest experimental set-up the temperature T of the sample is controlled by a computer program such that it changes linearly with time t (Fig. XVI.1a)

$$T = T_0 + \beta t \ (\beta > 0). \tag{XVI.4}$$

The pressure rise as a function of temperature T is then given by

$$p \propto \frac{-\mathrm{d}\theta}{\mathrm{d}t} = \frac{\overline{\sigma}}{\beta}\theta^n \mathrm{e}^{-E_{\mathrm{des}}/kT}, \tag{XVI.5}$$

where for the general case of a desorption process of order n, the occupation factor $\overline{f}(\theta)$ is assumed as θ^n (Sect. 10.5). For monomolecular and bimolecular desorption n equals 1 and 2, respectively. The measured pressure as a function of sample temperature (Fig. XVI.1b) reaches a maximum at a characteristic temperature T_{p} and decreases again when the surface coverage decreases by desorption. The pressure rise is determined by the exponential term in (XVI.5), whereas the decrease of $p(\propto \theta^n)$ also depends on the order of the desorption process. The temperature of the maximum of $p(T)$ is determined by

$$-\frac{\mathrm{d}^2\theta}{\mathrm{d}T^2} = \frac{\mathrm{d}}{\mathrm{d}T}(\overline{\sigma}\theta^n \mathrm{e}^{-E_{\mathrm{des}}/kT}) = 0. \tag{XVI.6}$$

Inserting the expression for $\mathrm{d}\theta/\mathrm{d}T$ (XVI.5), one obtains for an nth-order desorption process

$$\ln\left[T_{\mathrm{p}}^2 \frac{1}{\beta}\theta^{n-1}(T_{\mathrm{p}})\right] = \frac{E_{\mathrm{des}}}{kT_{\mathrm{p}}} + \ln\left(\frac{E_{\mathrm{des}}}{n\overline{\sigma}k}\right), \tag{XVI.7}$$

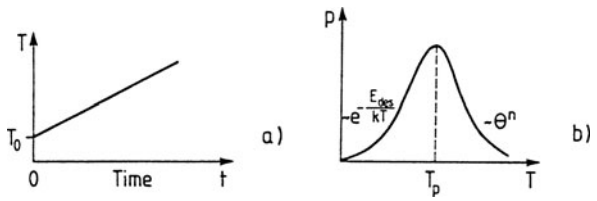

Fig. XVI.1 a,b Qualitative description of a Thermal Desorption Spectroscopy (TDS) experiment. (**a**) The sample temperature T is increased linearly with time t, starting from an initial value T_0. (**b**) Due to desorption the pressure in the UHV vessel increases and decreases again with increasing sample temperature. The initial increase is mainly determined by the desorption barrier E_{des}, whereas the pressure drop gives information about the order n of the desorption process

or for a simple monomolecular process

$$\ln(T_p^2/\beta) = \frac{E_{des}}{kT_p} + \ln\left(\frac{E_{des}}{\overline{\sigma}k}\right). \qquad \text{(XVI.8)}$$

With reasonable assumptions about the steric factor $\overline{\sigma}$ (XVI.7, XVI.8) are used to determine the desorption energy E_{des} by recording the p versus T dependence (Fig. XVI.1b).

From the mathematical form of the pressure (or desorption rate) versus temperature curve, it is obvious that only for a monomolecular process is the temperature of the maximum T_p independent of θ and thus also of θ_0, the initial coverage (Fig. XVI.2a). A shift of the desorption peak with an initial coverage variation indicates a desorption process of higher order as in Fig. XVI.2b [XVI.2].

Further information about the order of the process is obtained from the shape of the desorption curve [XVI.2]. Second-order curves are symmetrical with respect to T_p, whereas first-order desorption causes less symmetric bands (Fig. XVI.3).

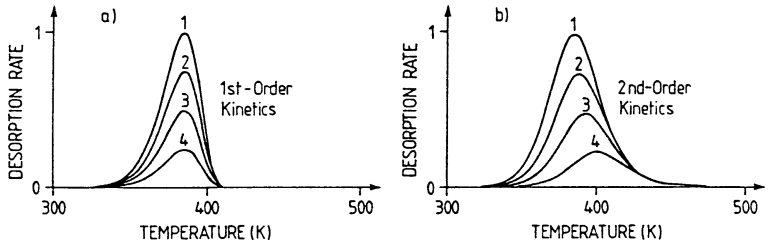

Fig. XVI.2 a,b Thermal desorption spectra, i.e. desorption rate (dimensionless) versus sample temperature T. For the calculation a desorption energy E_{des} of 25 kcal/mole and different fractional surface coverages have been assumed: (1) $\theta = 1.0$, (2) $\theta = 0.75$, (3) $\theta = 0.5$, (4) $\theta = 0.25$. The desorption process has been assumed to involve (**a**) first-order kinetics, and (**b**) second-order kinetics

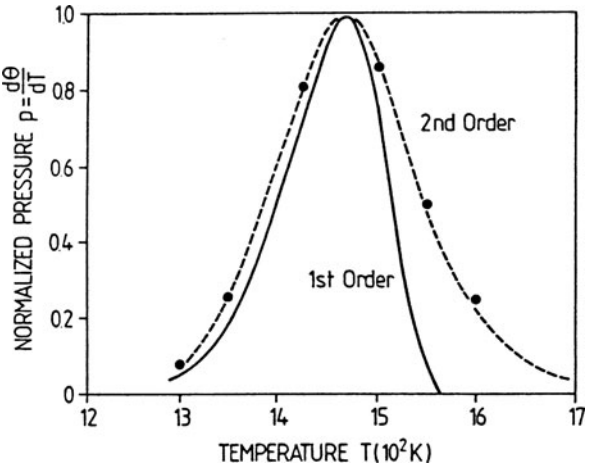

Fig. XVI.3 Normalized desorption rate as a function of temperature for a first-order ($E_{des} = 91.5$ kcal/mole) and a second-order ($E_{des} = 87.5$ kcal/mole) reaction, calculated for a linear temperature sweep. The experimental data (dark circles) are obtained from desorption experiments on the so-called β-phase of N_2 on W, adsorbed at 300 K [XVI.1]

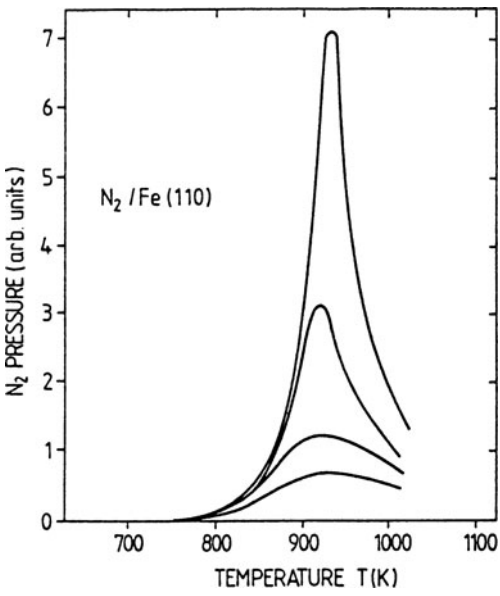

Fig. XVI.4 Thermal Desorption Spectra (TDS) of nitrogen (N_2) desorbed from a Fe(110) surface. The mathematical description in terms of a second-order process gives a desorption energy E_{des} of 7 eV per atom [XVI.3]

Another experimental example of second-order desorption in TDS is given in Fig. XVI.4, where the desorption of N_2 from Fe(110) surfaces is monitored [XVI.3]. The description in terms of a second-order process yields the information that nitrogen is adsorbed dissociatively and the desorption energy E_{des} is estimated to be roughly 7 eV per atom.

In another type of desorption experiment the surface bearing the adsorbate is irradiated and it is the incident energy that gives rise to desorption. Depending on the particular type of radiation one distinguishes several techniques:

- In *Ion Impact Desorption* (IID) ions of typically 100 eV primary energy, e.g. Ar ions, are accelerated onto the sample and adsorbate particles are desorbed by direct momentum transfer. Mass-spectroscopic detection generally reveals only the chemical nature of the adsorbate.
- In *Field Desorption* (FD) high electric fields ($\approx 10^8$ V/cm) are applied by a counter-electrode, e.g. in a field-ion microscope, and the desorbing particles can be made visible on a fluorescent screen. Local adsorption geometry is sometimes studied but energetic questions are rarely tackled by this method.
- In *Photodesorption* (PD) experiments light of sufficient photon energy (3–10 eV) is used to excite electrons from the adsorbate bond into antibonding orbitals. This disrupts the adsorption bond and leads to desorption. PD is usually accompanied by heat transfer and the effect is sometimes difficult to distinguish from thermal desorption.
- Of considerable importance in adsorption studies is *Electron Stimulated Desorption* (ESD). In this technique electrons with primary energies up to about 100 eV are incident on the adsorbate covered surface; the desorbing productes are either

detected mass-spectroscopically or one uses a multichannel plate array backed by a fluorescent screen to obtain a spatial image of the desorption direction of the removed particles. This technique of visualizing the angular distribution of the desorbing atoms or molecules is called ESDIAD (Electron Stimulated Desorption of Ion Angular Distributions). Figure XVI.5 shows a typical experimental set-up, which allows both mass-spectroscopic detection (ESD) and the collection of ESDIAD data [XVI.4]. Mass spectroscopy yields information about the chemical nature of the desorbing species, whereas detection of the angular distribution gives insight into the local geometrical arrangement of the adsorbed complex. Inversion of the bias at the Multichannel Plate (MCP) array enables the detection of electrons, i.e. the optical display of a diffraction pattern. This allows the simultaneous observation of the LEED pattern (Panel VIII: Chap. 4) of the adsorption system.

The theoretical description of ESD processes is based on two limiting cases. In the classical model of Menzel and Gomer [XVI.5] intramolecular excitations (indicated by the shaded area in Fig. XVI.6) within the adsorbed molecule lead to non-bonding and antibonding neutral or ionic final states. At the crossover points of the corresponding potential curves (Fig. XVI.6) the adsorbed molecule can change into the new state and might desorb. In the case of ion desorption an electron can be captured by tunneling from the solid to a desorbing particle.

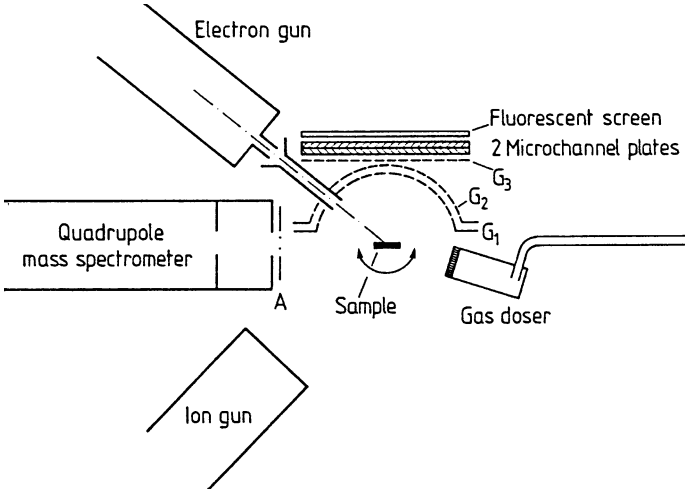

Fig. XVI.5 Schematic picture of an Electron Stimulated Desorption (ESD) and ESDIAD apparatus. The sample S can be rotated about an axis normal to the plane of the drawing. ESD ions are mass-analyzed in the quadrupole mass spectrometer, and ESDIAD patterns are displayed using the grid MicroChannel-Plate (MCP) plus fluorescent screen array. The radius of curvature of G_1 is 2 cm, and the active area of each MCP has a diameter of 4 cm. For most ESDIAD measurements typical potentials are $G_1 = G_2 = 0V$, $G_3 = -70$ V, MCP entrance: -700 V, MCP midpoint: 0 V, MCP exit: $+700$ V, fluorescent screen: $+3800$ V. Electron gun filament potential $V_f = -100$ V, crystal potential $V_B = 0$ to $+100$ V. Electron energy $E_e = e(|V_f| + |V_B|)$ [XVI.4]

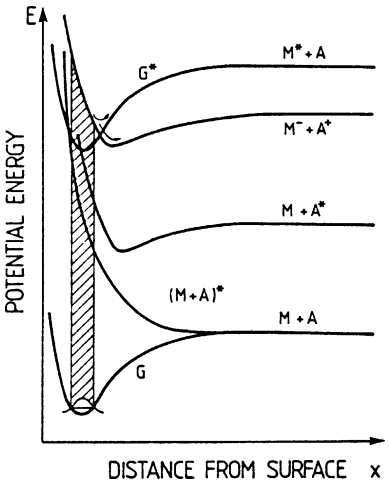

Fig. XVI.6 Potential energy diagrams for an adsorbate system. G: adsorbed ground state; $M^- + A^+$: ionic state; $(M + A)^*$: antibonding state; $M + A^*$: excited state of the adsorbate; $M^* + A$: adsorbate ground state with excitation energy in the metal (vertically shifted replica of G). The vibrational distribution in G and resulting ESD ion energy distribution are indicated [XVI.2]

This type of excitation, however, does not explain ESD results which have been observed on $TiO_2(001)$ surfaces on which tiny amounts of hydrogen were adsorbed (Fig. XVI.7) [XVI.6, XVI.7]. Under irradiation with quasi monoenergetic electrons of varying primary energy, thresholds in the desorption flux of H^+ and O^+ ions are observed near 21 eV and 34 eV, respectively. As is seen from additional double differentiated EELS measurements (inset), these energies correspond to the O(2s) and Ti(3p) core-level excitations. The interpretation of these desorption experiments on highly ionic materials involves the formation of core-level holes in the O(2s)

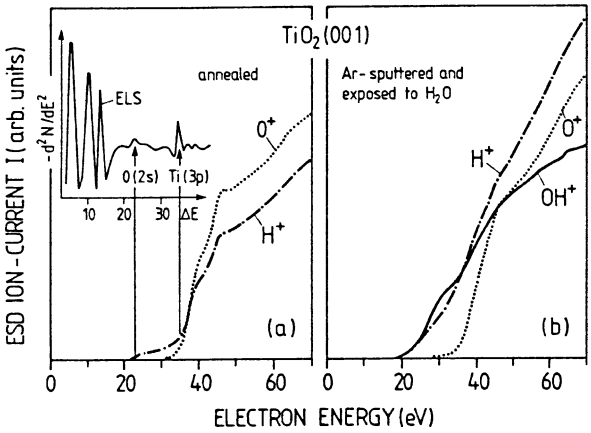

Fig. XVI.7 a,b Ion yields (O^+, H^+, OH^+) from Electron-Stimulated Desorption (ESD) measurements on: (**a**) a clean annealed $TiO_2(001)$ surface (the H^+ yield probably results from slight contamination); (**b**) an Ar-sputtered $TiO_2(001)$ surface after exposure to H_2O. For comparison, part (**a**) contains as an insert a second-derivative Electron Energy Loss Spectrum (EELS) of the same annealed surface. Its loss scale (ΔE) is identical with the scale of the ESD primary energy. Transitions from the O(2s) and Ti(3p) levels to the vacuum level are indicated [XVI.6]

and Ti($3p$) orbitals and subsequent interatomic transitions between the O and Ti core levels. In detail, primary electrons create a Ti($3p$) core hole, and owing to an interatomic Auger process an O($2p$) electron decays into the Ti($3p$) state, with the emission of a second or third O($2p$) electron to dissipate the energy released in the decay. This fast process is responsible for the relatively large charge transfer in the transformation of the O^{2-} lattice ion into O^{+}, which is observed in ESD. The H^{+} desorption spectrum exhibiting two thresholds (Fig. XVI.7) may be interpreted in terms of two types of hydrogen, that bonded to O and that bonded to Ti surface atoms. Energy-dependent ESD measurements can thus give detailed information about atomic-scale features of the electron-induced desorption process.

Experimental examples of the use of ESDIAD in the determination of an adsorption geometry are given in Fig. XVI.8. From TDS it is known that H_2O and NH_3, adsorb molecularly on the Ru(001) surface at 90 K. Irradiation by electrons with primary energies below 100 eV produces angularly-resolved desorption patterns of H^{+} ions, as shown in Fig. XVI.8b–d [XVI.4]. For low coverages a halo-type pattern is observed. Assuming that the desorbing H^{+} ions leave the surface along the direction of the intramolecular chemical bond, a low-coverage bonding geometry is derived in which the H_2O and NH_3 molecules are bonded with their O and N atoms closest to the surface. The orientation with respect to the 2D lattice planes of the surface is irregular or statistical. At increased coverages a hexagonal symmetry becomes visible in the ESDIAD patterns, which demonstrates that the molecular orientation

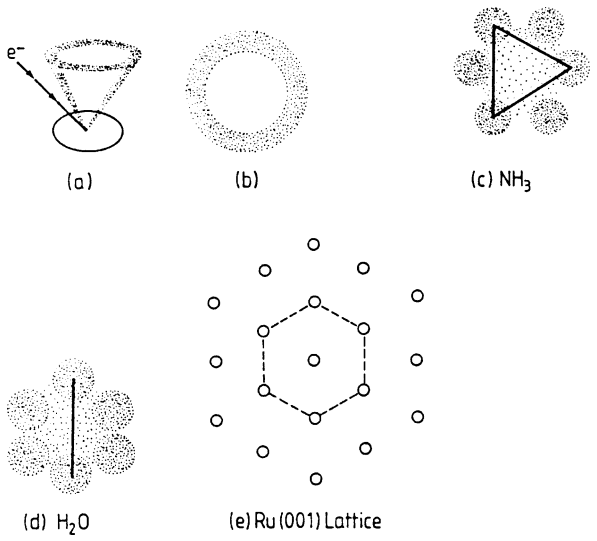

Fig. XVI.8 a–e Schematic ESDIAD patterns for H_2O and NH_3 adsorbed on Ru(001) at 90 K [XVI.4]. (**a**) Formation of hollow cone of H^{+} ions from adsorbed NH_3 and H_2O (at low coverages). (**b**) "Halo" H^{+} pattern characteristic of low coverages of NH_3 and H_2O. (**c**) Hexagonal H^{+} pattern characteristic of intermediate NH_3 coverages ($0.5 \leq \theta < 1$). (**d**) Hexagonal H^{+} pattern characteristic of intermediate H_2O coverages ($0.2 \leq \theta < 1$). (**e**) Ru(001) substrate with respect to the ESDIAD patterns above

is now in registry with the underlying substrate (Fig. XVI.8c–e). The molecules have lost one degree of freedom, the free rotation around an axis normal to the surface. With certain assumptions about the microscopic desorption process, ESDIAD thus allows detailed conclusions concerning the local adsorption geometry.

References

XVI.1 F.M. Lord, J.S. Kittelberger: Surf. Sci. **43**, 173 (1974)
XVI.2 D. Menzel: In *Interactions on Metal Surfaces*, ed. by R. Gomer, Topics Appl. Phys. Vol. 4 (Springer, Berlin, Heidelberg, 1974) p. 124
XVI.3 F. Bozso, G. Ertl, M. Weiss: J. Catalysis **50**, 519 (1977)
XVI.4 T.E. Madey, J.T. Yates: Proc. 7th Int'l. Vac. Congr. and Int'l. Conf. Solid Surfaces, Wien (1977)
XVI.5 D. Menzel, R. Gomer: J. Chem. Phys. **41**, 3311 (1964)
XVI.6 M.L. Knotek: Surface Sci. **91**, L17 (1980)
XVI.7 M.L. Knotek, P.J. Feibelman: Phys. Rev. Lett. **40**, 964 (1978)

Panel XVII
Kelvin-Probe and Photoemission Measurements for the Study of Work-Function Changes and Semiconductor Interfaces

The adsorption of atoms or molecules on a solid surface, i.e. the first steps of the formation of a solid–solid interface, is generally associated with a change of work function (Sect. 10.3), and on semiconductors also with a change in band bending (because of the formation of new interface states). These effects can be studied in situ both by photoemission spectroscopy (UPS and XPS; Sect. 6.3) and by Kelvin-probe measurements. The latter technique, in particular, is useful for work-function measurements on metal surfaces, where space-charge layer effects are negligible (spatial extension of some Ångstroms).

Kelvin probes for the determination of work-function changes consist of an electrode (usually point-like) which can be positioned in front of the surface being studied (Fig. XVII.1a). This counterelectrode is driven electromagnetically by a solenoid or by piezoceramics such that it vibrates with frequency ω against the sample surface. Sample and vibrating electrode are connected electrically through an ammeter (A) and a battery which allows a variable biasing (U_{comp}).

The principle of the work-function measurement becomes clear if we consider that for two solids [sample S and probe P] in electrical contact the electrochemical potentials, i.e. the Fermi energies $E_{\mathrm{F}}^{\mathrm{S}}$ and $E_{\mathrm{F}}^{\mathrm{P}}$, are equal in thermal equilibrium ($E_{\mathrm{F}}^{\mathrm{S}} = E_{\mathrm{F}}^{\mathrm{P}}$). Since in general the work function ($e\phi = E_{\mathrm{vac}} - E_{\mathrm{F}}$ is different for the sample surface and for the Kelvin probe, a so-called *contact potential* U^{SP} is built up between the sample and the probe.

Since

$$E_{\mathrm{F}}^{\mathrm{S}} = E_{\mathrm{vac}}^{\mathrm{S}} - e\phi^{\mathrm{S}} = E_{\mathrm{vac}}^{\mathrm{P}} - e\phi^{\mathrm{P}} = E_{\mathrm{F}}^{\mathrm{P}}, \tag{XVII.1}$$

the contact potential is obtained as

$$U^{\mathrm{SP}} = -\frac{1}{e}(E_{\mathrm{vac}}^{\mathrm{S}} - E_{\mathrm{vac}}^{\mathrm{P}}) = -(\phi^{\mathrm{S}} - \phi^{\mathrm{P}}). \tag{XVII.2}$$

Measurement of this contact potential therefore determines the difference in work function between the Kelvin probe and the sample surface. In an experimental set-up as in Fig. XVII.1 the voltage between sample and probe is

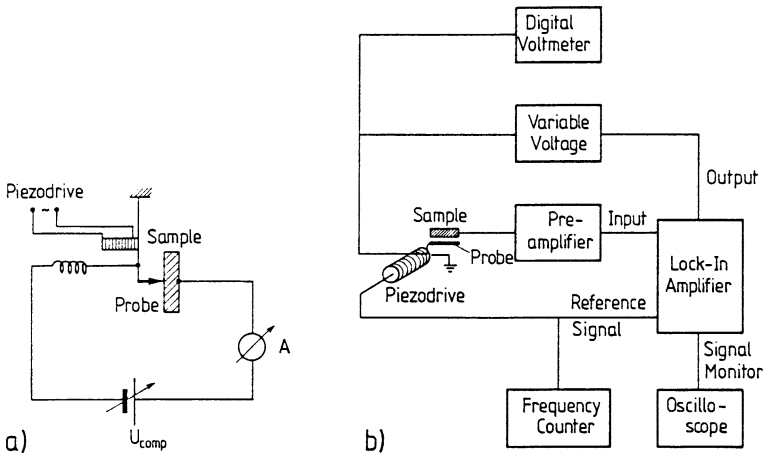

Fig. XVII.1 (**a**) Principle of a Kelvin probe measurement; the compensation voltage U_{comp} compensates the AC current driven by the vibrating probe. (**b**) Schematic circuit for the Kelvin probe measurement

$$U = -(\phi^{\text{S}} - \phi^{\text{P}}) + U_{\text{comp}}. \tag{XVII.3}$$

The capacitor formed by sample and probe thus carries a charge (C being the capacitance)

$$Q = C[-(\phi^{\text{S}} - \phi^{\text{P}}) + U_{\text{comp}}], \tag{XVII.4}$$

and the vibration of the probe electrode (frequency ω) gives rise to an oscillating current

$$I = \frac{\mathrm{d}Q}{\mathrm{d}t} = \frac{\mathrm{d}C}{\mathrm{d}t}[-(\phi^{\text{S}} - \phi^{\text{P}}) + U_{\text{comp}}]. \tag{XVII.5}$$

By means of the compensation voltage U_{comp} the oscillating current I is compensated to zero and the particular value of U_{comp} yields the difference in work function

$$U_{\text{comp}} = \phi^{\text{S}} - \phi^{\text{P}}. \tag{XVII.6}$$

For practical purposes Kelvin-probe measurements are usually performed by automatic compensating circuits, for example, of the type shown in Fig. XVII.1b. The AC current between sample and vibrating probe is amplified and detected phase-sensitively by a lock-in amplifier. The reference signal from the lock-in is also used to control the frequency of the AC voltage supplying the piezodrive. The DC output of the lock-in, which is proportional to its AC input amplitude, controls a variable voltage source which compensates the contact potential between sample surface and probe. The compensating voltage U_{comp} is read out by a digital voltmeter and gives directly the required contact potential difference (XVII.6).

If the work function $e\phi^{\mathrm{P}}$ of the reference electrode (probe) is known, the work function of the sample surface is determined. The method is readily applicable if the sample surface can be covered by an adsorbate without affecting the probe surface. This can be achieved, e.g., if the Kelvin probe can be removed during evaporation onto the sample surface (with geometrically well-defined beam). Difficulties arise when adsorption from an ambient is studied and the probe surface is exposed to the same gas atmosphere. The accuracy of Kelvin probe measurements is quite high. Relative changes in ϕ^{S} can be determined within error limits of about 10 meV. Absolute measurements, of course, depend on a knowledge of the work function of the probe. Absolute measurements are sometimes performed by means of comparison with well-defined surfaces for which the work function is known from other measurements. Two measurements are then needed, one on the known surface and one on the sample under study. The necessary exchange of the two samples in front of the Kelvin probe decreases the accuracy of the measurement considerably.

For semiconductor surfaces a knowledge of the work-function change $e\Delta\phi = e\phi' - e\phi$ due to adsorption does not give direct insight into atomic properties. The work-function change contains contributions due to band-bending changes and in addition a surface dipole contribution which may be described as a change of the electron affinity χ. These two contributions can be determined separately in a photoemission experiment with UV light (UPS) or X-ray excitation (XPS). According to Fig. XVII.2 an adsorption process giving rise to extrinsic Surface States (SS) in the gap and thus an upwards band bending (depletion layer) causes the work function $e\phi$ to change into

$$e\phi' = e\phi + eV_{\mathrm{S}} + e\Delta\phi_{\mathrm{Dip}}, \tag{XVII.7}$$

where V_{S} is the band bending (change in Fig. XVII.2); $e\Delta\phi_{\mathrm{Dip}}$ is a dipole contribution arising from the elemental dipoles of the adsorbed molecules or atoms (Δ) and may also include a change of the electron affinity $\Delta\tilde{\chi}$ due to a surface reconstruction during adsorption

$$e\Delta\phi_{\mathrm{Dip}} = \Delta + \Delta\tilde{\chi}. \tag{XVII.8}$$

The distinction between Δ and $\Delta\tilde{\chi}$ is rather arbitrary and can be avoided by using a single change of the electron affinity $\Delta\chi$, such that the change in the work function due to adsorption is given as in (10.17).

Figure XVII.2 is a schematic drawing of a photoemission experiment (UPS) in which electrons are emitted from occupied valence band states (of density given by shaded area) by irradiation with photons of energy $\hbar\omega$ and detected with a kinetic energy E_{kin}. The detected spectral distribution (also shaded) thus resembles the density of occupied states, but is superimposed on a background of true secondaries, which have undergone several inelastic processes on their way from the point of excitation to the solid surface. Since the probing depth in such an experiment is only a couple of Ångstroms (Sect. 6.3), small in comparison with the thickness of the space charge layer, the measured electron distribution yields information about the electronic band structure at the very surface. In the experiment the Fermi energy E_{F}

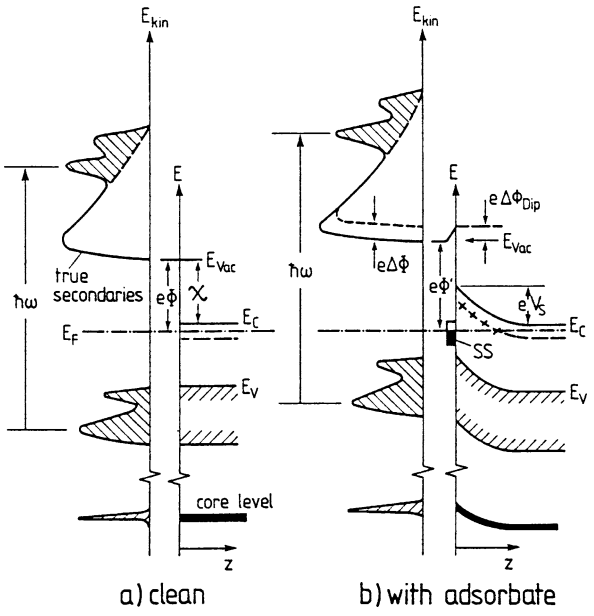

Fig. XVII.2 a,b Explanation of adsorbate-induced changes in the photoemission spectrum of a semiconductor: (**a**) Photoemission process on the clean surface of a semiconductor. Photons of energy $\hbar\omega$ excite electrons from the valence band (upper edge E_V) into empty states, from where they leave the crystal and are detected with a kinetic energy above the vacuum energy E_{vac}. True secondary electrons arise from multiple scattering events within the crystal. (**b**) An adsorbate induces extrinsic Surface States (SS) in the bulk band gap and an upwards band bending eV_S. This changes the work function from $e\phi$ to $e\phi'$. Simultaneously with the shift in valence and conduction band states, core level states also shift upwards in energy at the surface

is the general reference point (chemical potential of electrically connected sample and analyser) and all measured energies are related to this. E_F is usually determined at the end of the different measurements by evaporating a metal film onto the sample surface and determining the high energy onset of emission which, on a metal surface, is given by E_F.

As is evident from Fig. XVII.2 a change of work function $e\Delta\phi = e\phi' - e\phi$ is directly detected as a change of the energy width of the entire spectral distribution of the emitted electrons. The exact position of the low energy flank of the true secondaries with respect to the experimentally determined position of E_F gives the absolute values of the work functions $e\phi$ with and without adsorbate present. In principle, both the work-function and the band-bending changes due to adsorption can be separately determined. The high-energy flank of the distribution of emitted electrons corresponds to the upper valence-band maximum (for normal emission). A shift of this flank due to adsorption indicates a shift of the valence-band edge with respect to the Fermi level and thus a band-bending change ΔV_S (or V_S for initially flat bands as in Fig. XVII.2). This is only true if the adsorption process produces no new surface states in the gap. Such extrinsic gap states would modify the spectral distribution at the high-energy flank and the determination of any shift

of the onset would be impossible. A second possibility for determining a band-bending change is via a characteristic emission band that is clearly recognized as due to bulk states (rather than surface states, Sect. 6.3.3). If this spectral band does not change its shape significantly upon adsorption (due to new surface states in the neighborhood), its position can be determined with sufficient accuracy on the clean surface and after adsorption. An observed shift gives direct information about the band bending change (Fig. XVII.2). For example, the adsorption of metallic Sn on GaAs(110) surfaces has been studied by UPS in order to gain information about the Schottky-barrier formation (Fig. XVII.3). The emission band near 4.7 eV binding energy (marked by an arrow) shifts to lower binding energy (i.e., towards the Fermi level E_F) with increasing Sn coverage as does the emission onset corresponding to the upper valence band edge. This indicates an upwards band-bending change, i.e., the formation of a depletion layer on *n*-type material. A quantitative evaluation of the band bending is not possible from the shift of the emission onset since new metal-induced surface states cause a strong deformation of the spectrum. This is clearly seen from the plot in Fig. XVII.4. The information about the band bending change must be extracted from the energetic position of the bulk emission band (filled circles).

A similar procedure for investigating band-bending changes upon adsorption can also be performed by XPS on core-level emission bands, since these shift in the same way as valence states (Fig. XVII.2). Standard XPS equipment, however, does not usually offer sufficient energy resolution, and so optical monochromators are

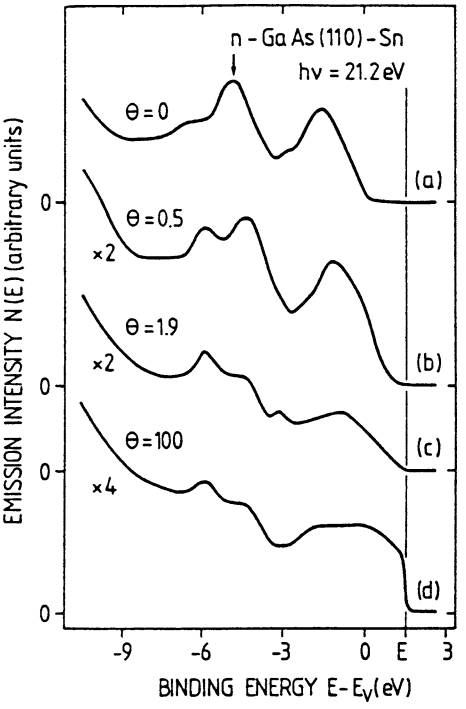

Fig. XVII.3 UPS electron energy distribution curves of a clean (**a**) and Sn covered (**b-d**) *n*-GaAs(110) surface taken with He I radiation ($h\nu = 21.2$ eV). The coverage θ is given in monolayers (1 ML contains $8.85 \cdot 10^{14}$ atoms/cm^2). The binding energy is defined relative to the energetic position of the valence band maximum at the clean surface. The arrow in spectrum (**a**) shows an emission band originating from bulk electronic states; its shift with coverage reflects the band bending change [XVII.1]

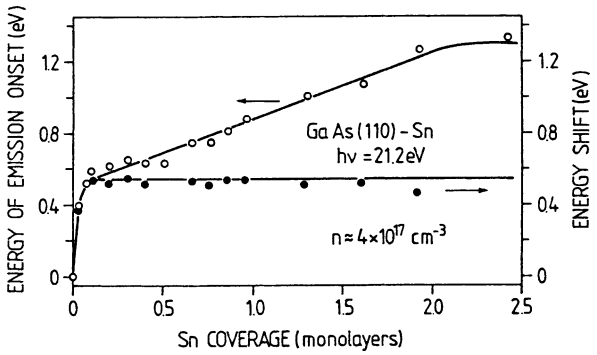

Fig. XVII.4 Position of the high-energy emission onset of the UPS spectra of Fig. XVII.3, relative to the position of the bulk valence-band maximum (open circles; left-hand ordinate) and energy shift of the GaAs valence-band emission peak (arrow in Fig. XVII.3) at 4.7 eV below VBM (full circles; right-hand ordinate) versus Sn coverage for *n*-GaAs [XVII.1]

needed. Furthermore, severe problems in the analysis of the data can occur when chemical bonding shifts (Sect. 6.3) are superimposed on the band-bending shifts.

Photoemission spectroscopy, in particular UPS, also yields the most direct way to measure band offsets (discontinuities) (Sect. 8.1) in situ between different epitaxy steps. The principle of the method is explained in Fig. XVII.5. On the same energy scale one plots the band structure of an uncompleted semiconductor heterostructure (a) together with the corresponding (kinetic) energy distribution of the emitted electrons (b). In an ideal case the clean surface spectrum of semiconductor I shows an emission onset which indicates the energetic position of its upper valence band maximum. After growing one or two monolayers of semiconductor II, a new shoulder

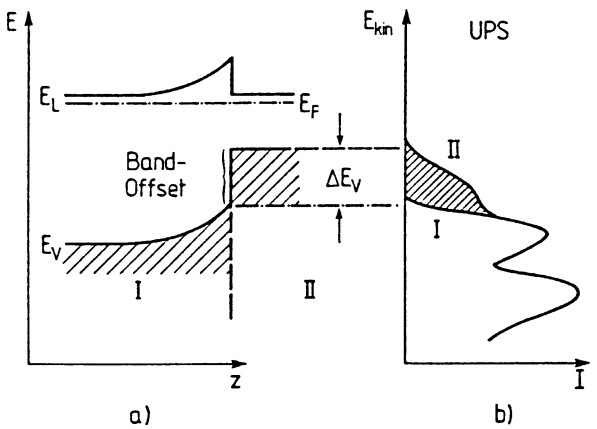

Fig. XVII.5 a,b Qualitative explanation of the determination of semiconductor valence band offsets ΔE_V by means of UV photoemission. On the clean surface of semiconductor I thin epitaxial layers of semiconductor II are grown (**a**) and the UPS spectra are measured in situ. (**b**) The shoulder II represents the valence band emission onset of semiconductor II on top of the valence band emission onset I of semiconductor I

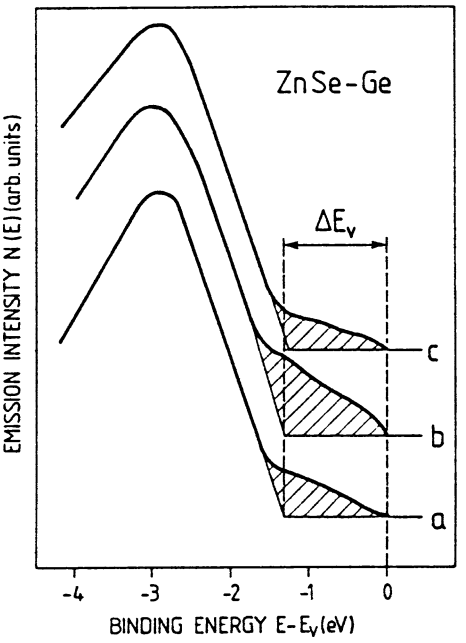

Fig. XVII.6 ZnSe-Ge photoemission spectra showing the valence band offset ΔE_V. These spectra were taken on unannealed, amorphous Ge overlayers (curve **a**) and on two different annealed Ge overlayers, exhibiting good LEED patterns (curves **b** and **c**). The spectra suggest that the order or disorder of the overlayer is not an important factor in ΔE_V for this particular system [XVII.2]

appears whose emission onset characterizes the upper valence-band edge of semiconductor II. The difference between the two thresholds is simply the valence-band discontinuity. It is clear that this technique only works when the valence-band edge of semiconductor II occurs at energies higher than that of semiconductor I.

Furthermore, the measurement can only be made on epilayers of thicknesses up to a couple of Ångstroms (information depth of UPS); but this is usually sufficient to allow the complete development of the band structure of semiconductor II. The method is illustrated in Fig. XVII.6 for Ge overlayers on a ZnSe substrate [XVII.2]. The energy of the new emission onset due to the Ge overlayer is insensitive to the crystallographic order of the Ge. An amorphous film exhibits the same band discontinuity as two other Ge overlayers which have been annealed and are crystalline.

In general, it should be emphasized that photoemission techniques give quite direct information about band-bending changes, work function and band discontinuities; but the accuracy in determining the absolute values is typically between 20 and 100 meV. This is usually inadequate for narrow gap semiconductor such as InSb or InAs, in particular for explaining the electronic properties of interfaces.

References

XVII.1 M. Mattern-Klosson, H. Lüth: Surf. Sci. **162**, 610 (1985)
XVII.2 G. Margaritondo, C. Quaresima, F. Patella, F. Sette, C. Capasso, A. Savoia, P. Perfetti: J. Vac. Sci. Technol. A **2**, 508 (1984)

Problems

Problem 10.1 A cesium ion (Cs^+) has an ionic radius of 3 Å. Calculate the approximate surface dipole moment for a (Cs^+) ion adsorbed on a tungsten (W) surface and discuss the result with respect to the observed work-function changes for Cs-adsorption on a W surface (Fig. 10.10).

Problem 10.2 Calculate the time at which 10% of the adsorption sites of a (100) W surface are occupied by nitrogen molecules, when the surface is exposed to an N_2 pressure of $2.67 \cdot 10^{-7}$ Pa at a temperature of 298 K. At this temperature the sticking probability is 0.55. The surface density of the adsorption sites amounts to $1 \cdot 10^{15}\,\mathrm{cm}^{-2}$.

Problem 10.3 Desorption studies of oxygen on tungsten (W) show that equal amounts of the gas are desorbed within 27 min at 1856 K, within 2 min at 1987 K and within 0.3 min at 2070 K. What is the activation energy for desorption of oxygen from W? What is the time needed for desorption of the sane amount of oxygen at the temperatures 298 K and 3000 K?

Problem 10.4 At 300 K, gas molecules have a sticking coefficient of $S = 0.1$ on a freshly prepared, clean semiconductor surface. The adsorption is thermally activated with a sticking coefficient $S \propto \exp(-E_{\mathrm{act}}/kT)$ and an activation energy per molecule of $E_{\mathrm{act}} = 0.1$ eV. How high are the adsorbate coverages after a one hour exposure at 300 K and at 70 K, respectively? Are the adsorbate coverages detectable by Auger Electron Spectrosopy (AES)?